

Vibrational Kinetics, electron dynamics and elementary processes in H₂ and D₂ Plasmas for Negative Ion Production: Modelling Aspects

M.Capitelli^{1,2,*}, R.Celiberto^{1,4}, O.De Pascale², P.Diomede¹, F.Esposito², A.Gicquel³, C.Gorse¹, K.Hassouni³, A.Laricchiuta², S.Longo¹, D.Pagano¹, M.Rutigliano², M.Cacciatore^{1,2}

¹*Department of Chemistry, University of Bari, Bari, Italy*

²*CSCP-IMIP(CNR), Sezione Territoriale di Bari, Bari, Italy*

³*LIMHP-CNRS, Université Paris Nord, Villetaneuse, France*

⁴*Politecnico di Bari, Bari, Italy*

**e-mail: mario.capitelli@ba.imip.cnr.it*

Abstract

Old and new problems in the physics of multicusp magnetic sources for the production of negative H⁻/D⁻ ions are presented and discussed. We emphasize particularly, in this kind of plasmas, both the vibrational and electron non equilibrium energy distributions, the role of Rydberg states in enhancing the negative ion production, the production of vibrationally excited states by the Eley-Rideal mechanism, and the enhancement of negative ion concentrations in pulsed discharges.

In appendix I recent cross sections calculations for elementary processes and the theoretical determination of hydrogen recombination probability on graphite surface are illustrated.

In appendix II two types of sources are modeled: the first one is a classical negative ion source in which the plasma is generated by thermoemitted electrons; in the second one, electrons already present in the mixture are accelerated by an RF field to sufficiently high energy to ionize the gas molecules.

1.Introduction

It is by now a well established fact that ITER program will use a negative ion beam for priming the fusion reaction. The research in this field started many years ago when Bacal *et al.* [1], [2] reported high fractions (<30%) of negative ions in electron beam sustained discharges in H₂/D₂. Since then, a lot of theoretical and experimental work was addressed to understand the physics of negative ions including their formation and their losses [3]-[11]. The synergy between theoretical and experimental work allowed the development of negative ion sources for different applications.

Nowadays, this synergy seems to be weakened because the researchers, who should build up the negative ion source for the different applications including that one for ITER, think the problem as a pure technological one. These researchers are experiencing procedures to improve the performances of the relevant sources, for both the plasma processes and the coupling of the external electrical power devices to the free electrons of the discharge. This is why we have assisted to the progressive substitution of volume sources to surface (cesium) ones as well as to the substitution of filament sustained discharges with rf ones [12]-[14]. In these sources, however, we have the same physics of negative ion production discussed in the

past, including many unresolved problems. Among them we remind 1) the experimental determination of the plateau of the vibrational distribution function, 2) the enhancement of negative ion concentrations by pulsed discharges, 3) the extension of the simulation to D₂ discharges, 4) the role of dissociative attachment from Rydberg states, and 5) the atom/molecule interaction with the surfaces.

These problems will be reviewed in this paper, by using old and new literature on the subject, with the hope to stimulate a new synergy between the researchers, in charge of the negative ion sources development for ITER program as well as for other applications, and the numerous European laboratories still active in plasma physics and plasma chemistry of negative ion sources.

1. Non-Equilibrium Plasma Kinetics

Different chemical-physical models were built in the last 20 years to describe the complex phenomenology occurring in multipole magnetic H₂/D₂ plasmas [3]-[11]. Time dependent and stationary approaches were used to this end.

The models include

- 1) the non equilibrium vibrational kinetics responsible for the population of vibrationally excited states,
- 2) an appropriate Boltzmann equation for describing the thermalization of electrons emitted by the filaments and accelerated by the applied voltage V_d ,
- 3) the dissociation kinetics for getting information about the concentration of atomic species,
- 4) the ion chemistry for determining the concentration of atomic and molecular positive ions,
- 5) the kinetics for the production and losses of negative ions including the dissociative attachment both from vibrationally excited states and Rydberg states.

A state to state approach is necessary for the characterization of the negative ion formation since the dissociative attachment occurs mainly from vibrationally excited states.

Points 1-5 were solved simultaneously due to the interdependence between all the quantities occurring in the different kinetics. To better understand the complexity of the kinetic problem we write, in implicit form, the equations for the first two steps of the complete kinetic scheme i.e., the vibrational kinetics and the Boltzmann equation (see also [8]).

For the vibrational kinetics we write [8].

$$\begin{aligned} \left(\frac{dN_v}{dt}\right) = & \left(\frac{dN_v}{dt}\right)_{e-V} + \left(\frac{dN_v}{dt}\right)_{E-V} + \left(\frac{dN_v}{dt}\right)_{V-V} + \left(\frac{dN_v}{dt}\right)_{V-T} + \\ & \left(\frac{dN_v}{dt}\right)_{e-D} + \left(\frac{dN_v}{dt}\right)_{e-I} + \left(\frac{dN_v}{dt}\right)_{e-da} + \left(\frac{dN_v}{dt}\right)_{e-E} + \left(\frac{dN_v}{dt}\right)_{wall} \end{aligned} \quad (1)$$

where each term on the right hand side represents the gain or the loss for the v -th vibrational quantum number under the influence of the relevant microscopic processes listed in Table I.

TABLE I
KINETIC PROCESSES

Symbol	Process
$e-V$	$e + H_2(v) \rightarrow e + H_2(w)$
$E-V$	$e + H_2(v=0) \rightarrow e + H_2(B^1\Sigma_u^+, C^1\Pi_u) \rightarrow e + H_2(w) + h\nu$
$V-V$	$H_2(v) + H_2(w) \rightarrow H(v-1) + H_2(w+1)$
$V-T_{mol}$	$H_2(v) + H_2 \rightarrow H_2(v-1) + H_2$
$V-T_{at}$	$H_2(v) + H \rightarrow H_2(v-1) + H$
$e-D$	$e + H_2(v) \rightarrow e + H_2^* \rightarrow e + H + H$ ($H_2^* = a^3\Sigma_g, e^3\Sigma_u^+, C^3\Pi_u, b^3\Sigma_u^+$) $e + H_2(v) \rightarrow e + H_2^* \rightarrow e + H + H^*$ $e + H_2(v) \rightarrow e + H_2^*(X^2\Sigma_u^+, X^2\Sigma_g^+) \rightarrow e + H^+ + H(1s)$
$e-I$	$e + H_2(v) \rightarrow e + H_2^+ + e$
$e-da$	$e + H_2(v) \rightarrow H + H^-$
$e-E$	$e + H_2(v) \rightarrow e + H_2^*$ ($H_2^* = E/F^3\Sigma_u^+, B^1\Sigma_u^+, D^1\Pi_u, B'^3\Sigma_u$)
Wall ₁	$H_2(v) \rightarrow H_2(w)$
Wall ₂	$H + H \rightarrow H_2(v)$
Wall ₃	$H_2^+ + e_{wall} \rightarrow H_2(v)$
$e-E_{at}$	$e + H \rightarrow e + H^*(n=2)$
$e-I_{at}$	$e + H \rightarrow e + H^+ + e$
$elastic_{mol}$	$e + H_2 \rightarrow e + H_2$
$elastic_{at}$	$e + H \rightarrow e + H$

The Boltzmann equation can be written as [8]-[10]

$$\frac{\partial n(\varepsilon, t)}{\partial t} = -\left(\frac{\partial J_{el}}{\partial \varepsilon}\right)_{e-M} - \left(\frac{\partial J_{el}}{\partial \varepsilon}\right)_{e-e} + In + Ion + Sup + S - L \quad (2)$$

where $-(\partial J_{el}/\partial \varepsilon)_{e-M}$ accounts for the flux of electrons along the energy axis due to elastic collisions, $-(\partial J_{el}/\partial \varepsilon)_{e-e}$ for that due to electron-electron Coulomb collisions, and the other terms correspond to inelastic (In), ionizing (Ion) and superelastic (Sup) collisions and electron losses (L) due to recombination either in gas phase or on the walls (see also table I). The term

S characterizes the source term and corresponds to the injection of electrons through the hot filaments and reads as:

$$S = I_d / (V e \Delta \varepsilon) \quad (3)$$

where I_d is the discharge current, V is the plasma volume, e is the electron charge and $\Delta \varepsilon$ is the energy spreading of the injected electrons.

A complete description of the plasma kinetics of negative ion sources requires a self-consistent coupling between the heavy particle kinetics and the electron one. This coupling occurs as heavy particle density evolution depends on the rate coefficients of electron processes whereas the electron energy distribution function *EEDF* turns to be a function of the distribution of heavy particles. For the i -th electron process, the rate coefficient k_i^e depends on the related cross section $\sigma_i(\varepsilon)$, with threshold energy ε_{th} , on the electron velocity $v(\varepsilon)$, and on the electron distribution $n(e)$ through

$$k_i^e = \int_{\varepsilon_{th}}^{\infty} \sigma_i(\varepsilon) v(\varepsilon) n(\varepsilon) d\varepsilon. \quad (4)$$

EEDF is governed by the electron Boltzmann equation, that describes the time evolution of the electrons with energy between ε and $\varepsilon + d\varepsilon$. It takes into account different terms involving the flux of electrons, in the energy space, due to various contributions. Some of the terms, appearing in the Boltzmann equation, are characteristic of the system we are investigating.

Similar equations describe both the atom and the positive and negative ion concentrations.

State to state cross sections entering in the kinetics have been discussed in the past by several authors. More recently a further effort, in improving the data base, has been reported by Celiberto *et al.* [15], [16] and by Fabrikant *et al.* [17] for electron molecule cross sections, by Esposito *et al.* [18] for H-H₂(v) cross sections, by Takagi [19] for dissociative recombination of different ions and by Wang and Stancil [20] for ion-molecule charge transfer and rearrangement. Details of the new calculations performed by our group are reported in Appendix 1 [95].

3. Non Equilibrium Vibrational Distributions

The vibrational distribution of H₂/D₂ molecules plays a determinant role in the formation of the negative ions since the dissociative attachment cross sections increase by many orders of magnitude with the increase of vibrational quantum number. This point stimulated and is still stimulating a lot of experiments for the determination of the whole vibrational distribution of H₂ and D₂ in the plasmas.

The first attempts used CARS [21] (Coherent Anti-Stokes Raman Spectroscopy) and REMPI [22] (Resonant Enhanced Multiphoton Ionization) techniques obtaining the first part of the vibrational distributions. As an example Fig. 1a-b [8] reports the experimental (a) and the theoretical (b) vibrational distributions N_v of H₂ up to $v = 5$ for different pressures p ($I_d = 10$ A, $V_d = 100$ V), whereas Fig. 2a-b [8] reports the same quantities for different discharge currents I_d ($p = 7.5$ mtorr, $V_d = 100$ V). In general, we observe a qualitative agreement between the theoretical and experimental values, even though the theoretical vibrational distributions are higher than the experimental ones. The most critical point, in this comparison, is the apparent quasi Boltzmann behavior of the experimental vibrational distributions against the clear appearance of the onset of a plateau, from $v = 3$ on, in the corresponding simulations. A quasi-Boltzmann vibrational distribution was also experimentally detected, at the Lawrence Berkeley National Laboratory [23] up to $v = 8$, by vacuum ultraviolet-laser absorption spectroscopy, in a source with $I_d = 24$ A and $p = 8$ mtorr (see also [24] for the corresponding theoretical study).

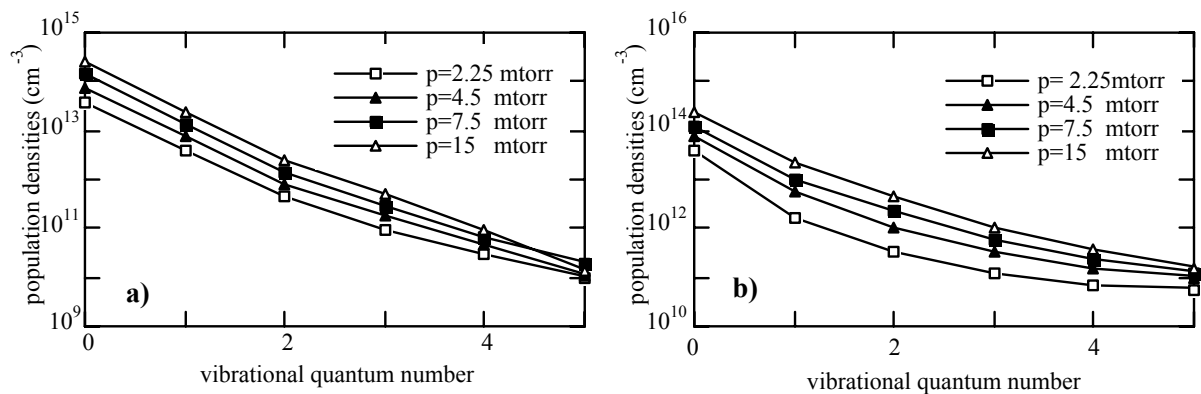


Fig. 1. A comparison between experimental (a) and theoretical (b) vibrational distributions at several pressures p [8].

It should also be noted that REMPI technique has been used by Robie *et al.* [25] for getting information on vibrational quantum number up to $v = 11$.

Vacuum ultraviolet absorption spectroscopy, used for the first time by Graham [26], is still in use in different laboratories [27], [28] to get information about high lying vibrational levels. More recently Dobele *et al.* [29], [30] were able to detect the vibrational distribution of H₂ up to $v = 13$ in a magnetic multipole plasma source, by laser-induced fluorescence with vacuum ultraviolet radiation, unambiguously showing the plateau in the vibrational distributions (see Fig. 3) as predicted by the theoretical results. We believe that this technique will open new interesting perspectives in the experimental determination of the vibrational distribution of H₂/D₂ systems.

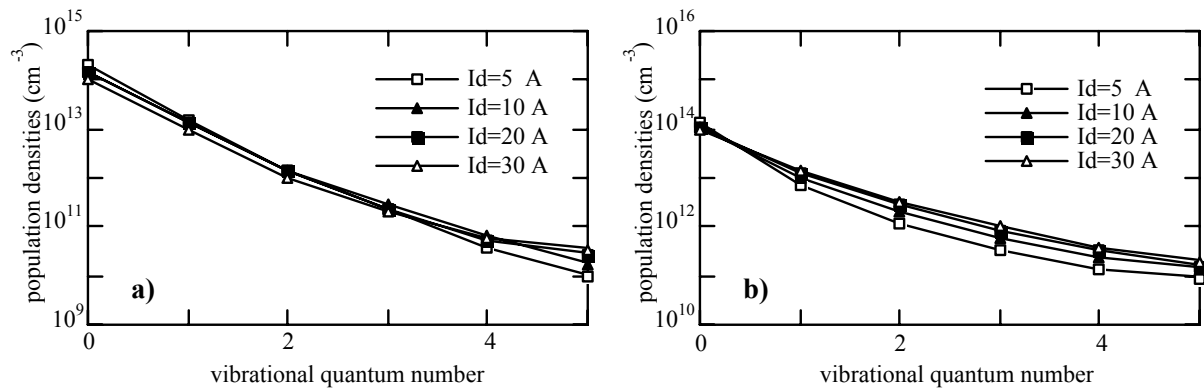


Fig. 2. A comparison between experimental (a) and theoretical (b) vibrational distributions at several discharge currents I_d [8].

3. Pulsed discharges

The time dependent simulation of multipole discharges showed that, switching on the discharge, both negative ion $n(H^-)$ and atom $n(H)$ densities rise with time [6]-[8]. However, at around 100 μ s, the negative ion density reaches a maximum, then decreases and saturates. This behavior was explained with the increased importance of associative detachment in collision with atoms, the density of which continues to rise. If, in a repetitive discharge, the current would be switched off as soon as the $n(H^-)$ density reaches its maximum value and for a period sufficiently long to affect the atom density, one would obtain a higher mean value of $n(H)$.

It should be noted that this procedure is correct as long as the atom life time, controlled by surface recombination, is shorter than that of either negative ions or vibrationally excited molecules. A second aspect of discharge modulation is related to the primary energetic electrons. As soon as the discharge is switched off their production stops and their density rapidly drops. Then also the fast electron detachment, one of the main actor in $n(H^-)$ destruction processes, is halted. A third aspect is linked to the temporal behavior of the low

energy part of *EEDF* which can find a temporal window, in the post-discharge, for increasing the dissociative attachment rates.

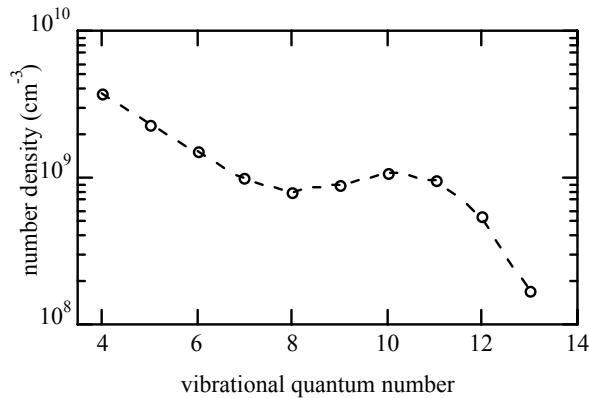


Fig. 3. Experimental vibrational distribution N_v measured in a H_2 multicusp source ($p = 11.25$ mtorr, $I_d = 0.5$ A, $V_d = 100$ V), adapted from [29].

Because of the similarity with the magnetic filter, in which there is a separation between fast and slow electrons, Hopkins and Mellon [31] called “temporal filter” the procedure of separating in time the required hot and cold electron distributions.

Different experiments [31]-[35] show the enhancement of $n(H)$ in the post discharge regime. Fig. 4 reports that one performed by Hopkins and Mellon which shows an enhancement by a factor 3 in the extracted H^- current. Note that the enhancement lasts for about 200 μs . Similar results (enhancement by a factor 2.5, time duration of about 100 μs) were obtained by Mosback *et al.* [34], who also developed a phenomenological model to explain the experimental results, and by Fukumasa and Shiroda [35] (enhancement by a factor 4 and duration of approximately 100 μs). On the other hand the code developed in Bari was used [36] to qualitatively reproduce the complex phenomenology of pulsed discharges. The results are summarized in Figs. 5a-d [36]. In particular Fig. 5a reports the relaxation of *EEDF* at several times t_{pd} in the post discharge. We can see that the relaxation of *EEDF* is such to increase the number of electrons with small energy, enhancing those rate coefficients characterized by a small threshold energy. In particular the dissociative attachment rates, from highly vibrational excited states, can increase during the relaxation as can be appreciated from Fig. 5b. Note that in D_2 system this behavior occurs for $v > 12$. On the other hand, Fig. 5c shows the relaxation of the vibrational distribution N_v , that starts decreasing after 100 μs . The D^- maximum, in the post discharge, can take place due to a favorable interplay between the relaxation of *EEDF*, and therefore of the dissociative attachment rates, the relaxation of N_v and the decrease of D^- losses in the post discharge regime. This is indeed the case as reported in Fig. 5d that shows the time dependence of negative ion concentration under discharge and

post discharge conditions. We can see, that when the discharge is switched off, a slight increase of D^- concentration appears, the effect being enhanced by reducing the vibrational losses on the metallic walls.

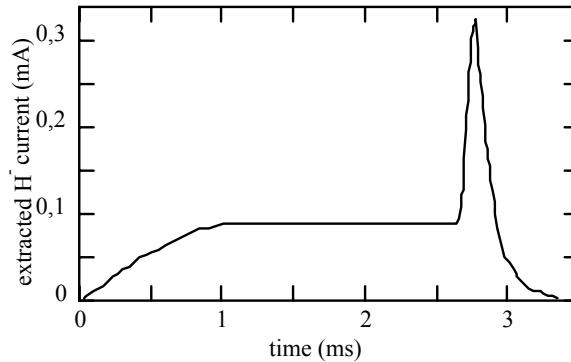


Fig. 4. Extracted H^- current in a pulsed hydrogen discharge with a $2.7 \mu s$ pulse length and a 87 Hz repetition rate ($p = 2.4$ mtorr, $I_d = 15$ A) [31].

The calculated negative ion concentrations are in line with the experimental results even though further improvements in the models must be done to obtain a better agreement with the experimental results.

Future improvement in pulsed discharges can be achieved by coupling numerical and experimental efforts.

5. D_2 Plasmas

Modeling of D_2 plasmas received and is receiving less attention in the hope that the results for H_2 plasmas can be extended to D_2 ones. An attempt in this direction was presented some years ago by Gorse *et al.* [37] which applied the self-consistent model discussed in section II to D_2 plasmas. Table 1 of [37] reports the elementary processes and the sources of the corresponding cross sections introduced in the simulation. A sample of results has been reported in Figs. 6-9. In particular, Figs. 6a and 6b compare stationary *EEDF* and vibrational distributions, in the same plasma conditions, for H_2 and D_2 . To understand the form of *EEDF* we must remember that in the multicusp magnetic discharges electrons are emitted by filaments and accelerated by the applied voltage V_d . The multicusp magnetic field is such to increase the confinement time of the electrons in the source. As a result the discharge is sustained by an electron beam that collides with the target gas. The resulting *EEDF*, obtained by the solution of the Boltzmann equation, is therefore typical of the degradation spectra of an electron beam through elastic (electron-molecule, electron-atom and electron-electron), inelastic (electronic dissociation and excitation), superelastic (collisions of electrons with

vibrationally excited states) and ionization collisions. So we can see the electron peak located at about 110 eV, followed by the long plateau caused by ionization and inelastic losses ending with the low energy bulk electrons, that represent the electrons at the final stage of their energy degradation. Note that the smooth plateau extending from 20 to 100 eV is due to electron-electron collisions that contribute to fill the depressions between maxima arising from ionizing and inelastic collisions [6], [9], [10].

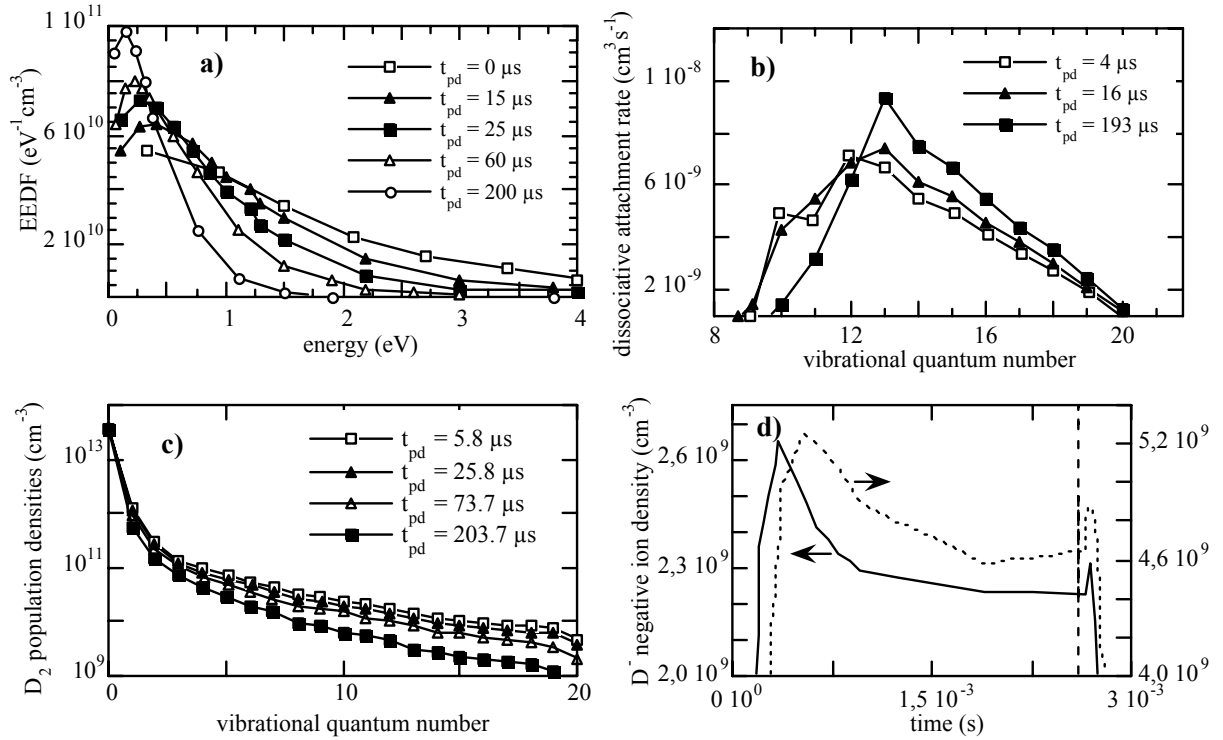


Fig. 5 Relaxation of several quantities ($EEDF$ (a), e-da rate coefficient (b), N_v (c), D^- density (d)) in the D_2 post-discharge regime (see text). In Fig. 5d, the dashed line has been obtained by decreasing by a factor 8 the rate coefficient for the deactivation of vibrationally excited molecules on the metallic walls, the vertical dashed line indicating the onset of the post-discharge regime [36].

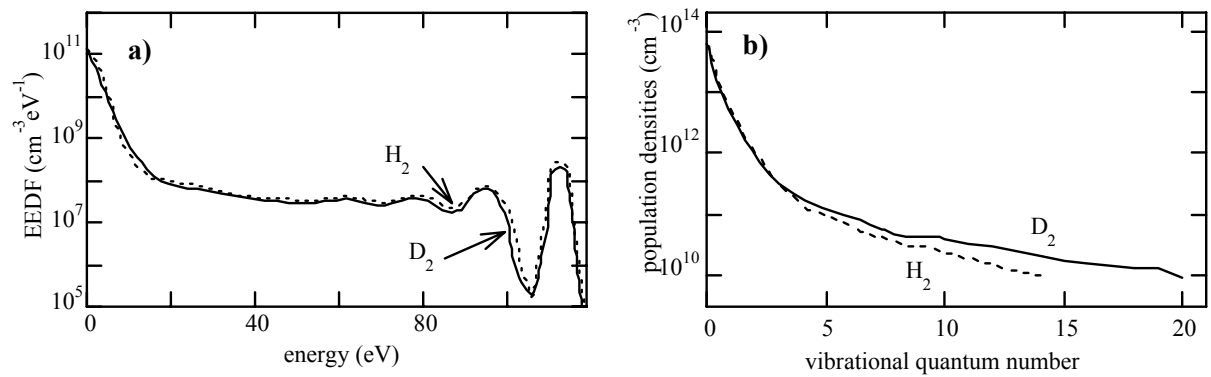
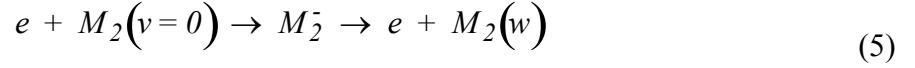
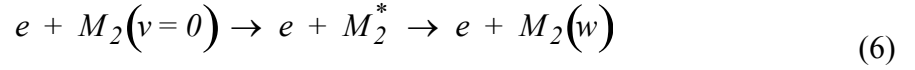


Fig. 6. Theoretical $EEDF$ (a) and N_v (b) in H_2 and D_2 multicusp sources ($p = 4.5$ mtorr, $I_d = 10$ A, $V_d = 115$ V, plasma potential $V_p = 2.9$ V) [37].

It should be noted that the theoretical *EEDF*, obtained by the solution of the Boltzmann equation, has been experimentally reproduced by using Langmuir probe technique [38], [39]. Concerning the form of the vibrational distribution (Fig. 6b), we can note a strong decay in the concentration of the first few levels followed by a long plateau. This behavior depends on the microscopic processes acting in the plasma and on their dependence on the vibrational quantum number. In particular the low energy part of the vibrational distribution depends on *e-V* rates



that strongly decrease with the increase of the vibrational quantum number v , while the long plateau is due to *E-V* rates



that present a weak dependence on the final vibrational quantum number.

The differences between H₂ and D₂ are quite small, specially in the *EEDF* behavior. The divergence in the vibrational distribution is mainly due to the differences in the vibrational energies of the two isotopes. This last point is responsible for the different behavior of the dissociative attachment rates in the two gases (Fig. 7).

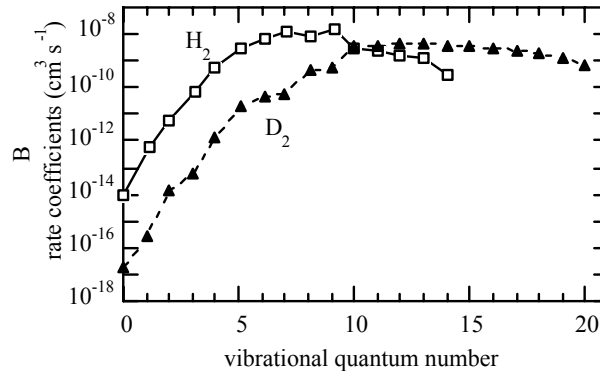


Fig. 7. Dissociative attachment (e-da) rates versus vibrational quantum number for H₂ and D₂ molecules (same conditions as Fig. 6) [37].

Again, we can see a similar behavior in the two systems but shifted to higher ν for D₂. Note also the strong dependence of the dissociative attachment rates on the vibrational quantum number, as already pointed out.

Figs. 8a-d and 9a-d show a comparison of different quantities (ne , Te , $[D]/[H]$, $[D^-]/[H^-]$) as a function of the pressure p and of the current intensity I_d . All these quantities increase by increasing pressure and current intensity, the only exception being represented by the behavior of electron temperature Te versus p at fixed I_d . In this case Te decreases as a function of p since the increase of inelastic losses, with the pressure, is such to cool the temperature of the bulk electrons.

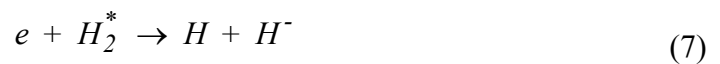
It should be noted that the electron temperature values Te , that are calculated by the slope of $EEDF$ in the low part of the distribution, in D₂ overcome the corresponding ones in H₂, the reverse being true for atom and negative ion concentrations and for the electron density ne . The reported trends are in qualitative agreement with the experimental ones reported by different authors [40], [41]. The experimental results have been obtained in multicusp magnetic plasmas operating under conditions slightly different from the calculations reported in the relevant figures. Note also that the differences, in the negative ion production in H₂ and D₂ plasmas, tend to disappear when comparing the extracted D⁻ and H⁻ currents corrected for the different ion mobilities.

In general the reported results seem confirm a small isotopic effect in the different plasma quantities.

Before concluding this section we want to point out that improvement in the cross sections for both H₂ and D₂ systems has been obtained in these last years [15]-[20] These new information should be included in future modeling of H₂ and D₂ plasmas.

6. Rydberg States

So far we have considered the dissociative attachment from vibrationally excited states as the mechanism for generating H⁻ ions. Recently, however, Pinnaduwa *et al.* [42], [43] proposed a new mechanism for producing negative ion based on the dissociative attachment on Rydberg states



where H_2^* represents a generic Rydberg state.

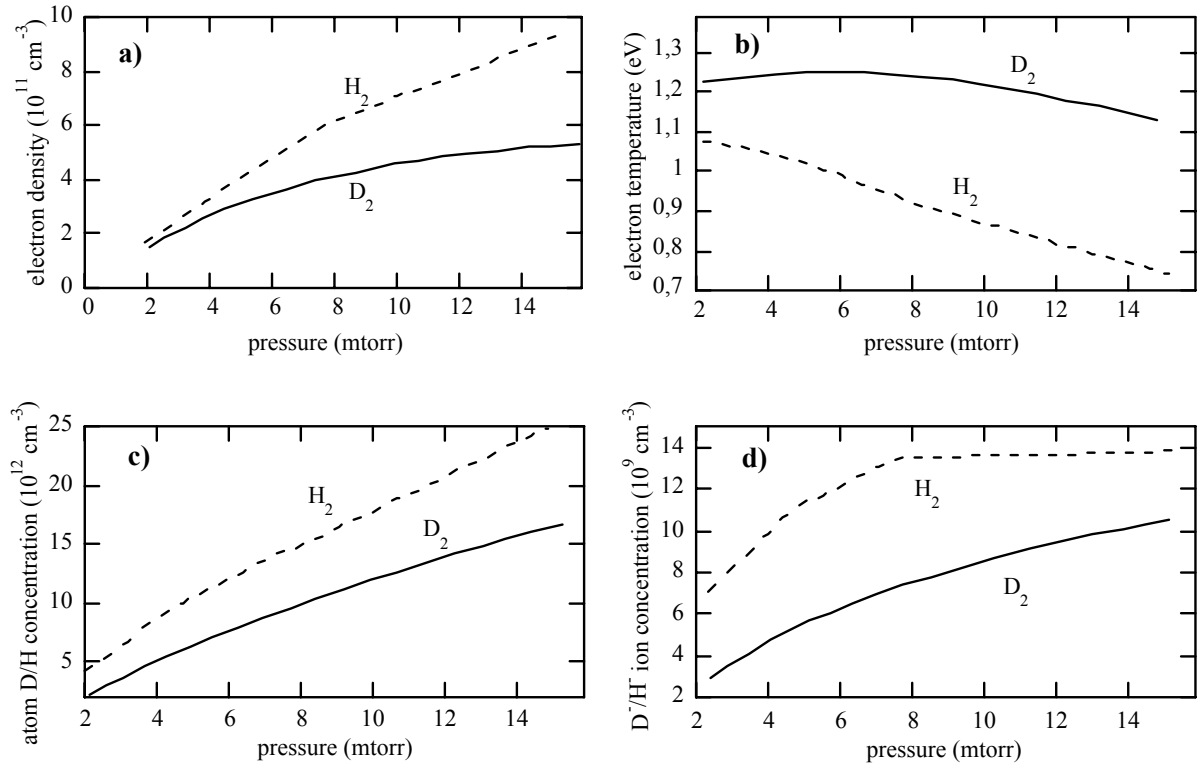


Fig. 8. The behavior of electron density ne (a), electron temperature Te (b), atomic concentration $[H]/[D]$ (c), and negative ion concentration $[H^-]/[D^-]$ (d), for H₂ and D₂ systems versus pressure p ($I_d = 10 \text{ A}$, $V_d = 115 \text{ V}$) [37].

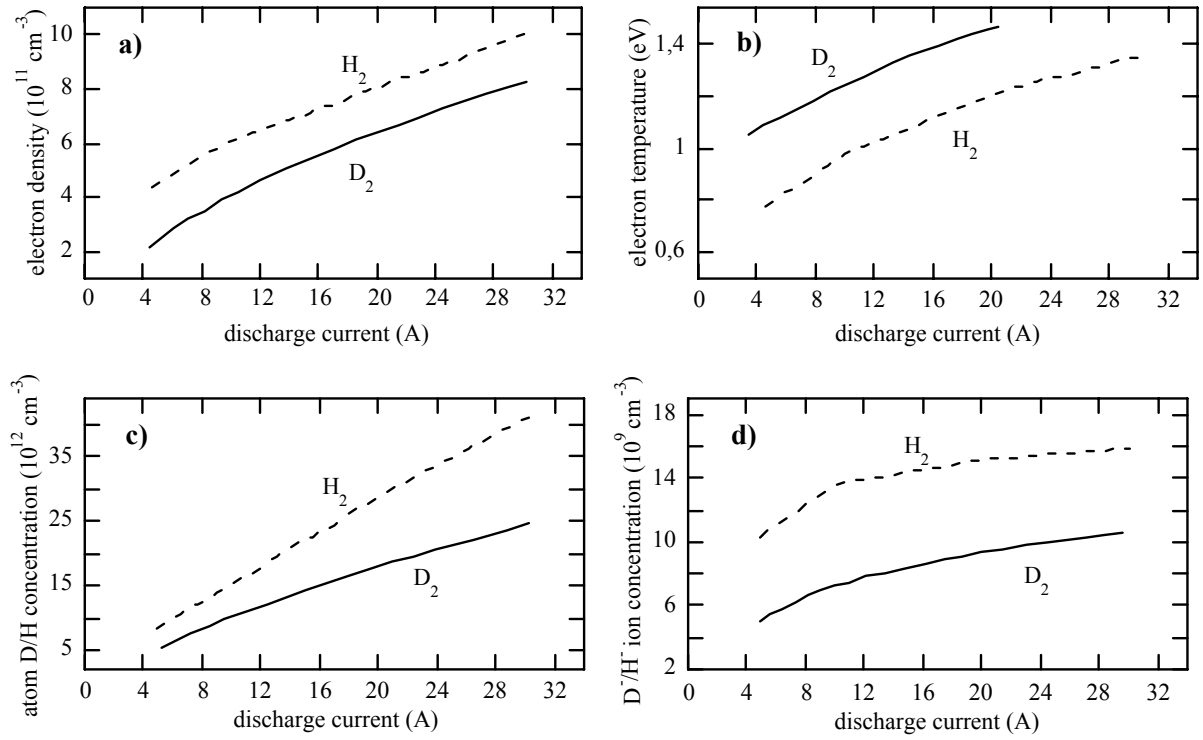


Fig. 9. The behavior of electron density ne (a), electron temperature Te (b), atomic concentration $[H]/[D]$ (c), and negative ion concentration $[H^-]/[D^-]$ (d), for H₂ and D₂ systems versus current I_d ($p = 7.5 \text{ mtorr}$, $V_d = 115 \text{ V}$) [37].

In a first paper, Pinnaduwege *et al.* [42] found an experimental value of $10^{-6} \text{ cm}^3 \cdot \text{s}^{-1}$ for the corresponding rate. A new value of $6 \cdot 10^{-5} \text{ cm}^3 \cdot \text{s}^{-1}$ was found by the same group in a subsequent publication [43]. The first value, i.e. $10^{-6} \text{ cm}^3 \cdot \text{s}^{-1}$, was used by Nagpal and Garscadden [44] in a simplified kinetic scheme



for estimating the concentration of negative ions through this mechanism. Insertion of this channel gives an enhancement of negative ion concentration by a factor 10 as compared with the concentration of negative ions obtained by the dissociative attachment mechanism from vibrationally excited states. This result was also confirmed, even though to a minor extent, by Gorse *et al.* [45] by introducing the channel in the self-consistent model previously described. The weakness of Nagpal and Garscadden model was in the selection of a lumped electron molecule cross section for populating the H_2 Rydberg states as well as for considering a value of 10^{-6} s for the lifetime A of the Rydberg states. The cross section for the excitation of Rydberg states was about $2.4 \cdot 10^{-17} \text{ cm}^2$ at 40 eV.

This kind of weakness has been discussed by Hiskes [46] who developed a collisional radiative model for the Rydberg states by using an elegant kinetic scheme. The major criticism of Hiskes was about the lifetime of Rydberg states used by Nagpal and Garscadden. According to the Hiskes treatment, the lifetime of $n = 3$ and $n = 4$ electronically excited states of molecular hydrogen should be decreased by a factor 100 i.e., $A = 10^{-8} \text{ s}$, thus reducing the importance of negative ion formation from the Rydberg mechanism by a factor 100. Hiskes' analysis ruled out the importance of the Rydberg mechanism until Pinnaduwege *et al.* reported a new experimental value of the attachment rate over Rydberg states 60 times higher than that one used by Nagpal and Garscadden, by Gorse *et al.* and by Hiskes. Using this new value, together with the arguments of Hiskes about the lifetime of Rydberg states, one should find a production of negative ions through the Rydberg mechanism of the same importance as that one coming from the dissociative attachment to vibrationally excited states.

This point has been confirmed in a recent study by Hassouni *et al.* [47], who have used the more recent dissociative attachment rates from the Rydberg mechanism, in a self-consistent kinetic model, including also a collisional radiative model to describe the electronically excited states of molecular hydrogen. For typical multicusp magnetic conditions, Hassouni *et al.* found an enhancement of the negative ion concentration by a factor 2.7, when the Rydberg state dissociative attachment mechanism was inserted in the complete model.

TABLE II

Electronically excited molecular state distributions in magnetic multicusp plasma

n	3	4	5	6	7	>4
$H_2^{*a)}$ (10^6 cm^{-3})	13.9	3.8				7,4
$H_2^{*b)}$ (10^6 cm^{-3})	24.0	11.0	4.6	2.0	0.85	8.3

^{a)} adapted from [47]
^{b)} adapted from [46]

It should be also noted that the concentrations of Rydberg states calculated by Hassouni *et al.* are in satisfactory agreement with the values found by Hiskes, in slightly different operating conditions, (see Table II). These new results indicate that the Rydberg mechanism can not be ruled out as suggested by Hiskes.

More accurate results can be obtained in the future, by inserting a scaling law for the dissociative attachment from Rydberg states, as a function of the principal quantum number n of the Rydberg state, as well as a better description of the population density of Rydberg states. An approximate scaling law, for dissociative attachment, as a function of the principal quantum number of the Rydberg state, has been proposed by Pinnaduwaage *et al.* [48] in the form

$$k_{da}(n) = 10^{-8} n^{7/2} \text{ cm}^3 \cdot \text{s}^{-1} \quad (11)$$

In this case, the Rydberg states responsible for electron attachment correspond to those with $n > 12$. We can compare the two dissociative mechanisms, from Rydberg and vibrationally excited states, in the form

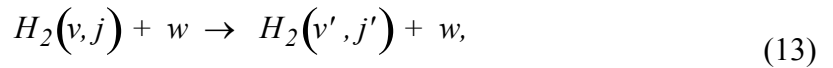
$$6 \cdot 10^{-5} \sum_{n>12} H_2(n) = 10^{-8} \sum_{v>4} H_2(v) \quad (12)$$

where we have assigned an upper limit to the rate of dissociative attachment from vibrationally excited states of the order of $10^{-8} \text{cm}^3 \cdot \text{s}^{-1}$. Taking into account a concentration of vibrationally excited states, on the plateau of the vibrational distribution, in the order of 10^{10} - 10^{12}cm^{-3} , we can estimate that Rydberg states with $n>12$ can be important for negative ion production when their concentrations are in the range $1/6 \cdot 10^7$ to $1/6 \cdot 10^9 \text{cm}^{-3}$.

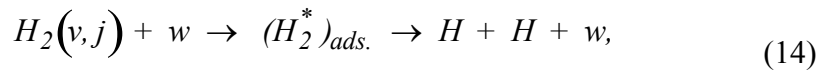
7. Wall effects

Plasma wall (w) interactions are of paramount importance for determining the non equilibrium vibrational distribution of $H_2(v)/D_2(v)$ species. We focus our attention on the following processes [49]

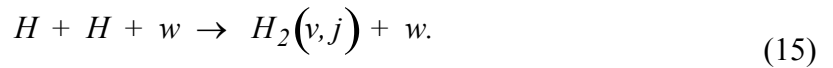
- vibrational (v) and rotational (j) relaxation in inelastic collisions



- dissociative chemisorption of vibrationally and rotationally excited molecules



- hydrogen atom recombination



The first two processes destroy vibrationally excited molecules, the reverse being true for the third process.

Pioneering work of Karo *et al.*, on the deactivation of vibrationally excited states on an iron surface, showed quite high accommodation coefficients. Their classical dynamical calculations were inserted in the codes of negative ion production by Gorse *et al.* [7], [8]

$$(dN_v/dt)_{wall} = (1/4) (A_0/V) \bar{v}_{H_2} \left(\sum_v (N_v/(vb(v))) - (N_v/b(v)) \right) \quad (16)$$

where A_0/V is the ratio between the total surface and the volume of the container, \bar{v}_{H_2} the mean velocity of H_2 molecules. The wall collision parameter $b(v)$ for deactivation of v th vibrational level ranges continuously from the value $b(v=1) = 4$ to $b(v=14) = 1$; molecules belonging to a particular vibrational level are assumed to be deactivated toward each lower level with the same probability.

More detailed and extensive molecular dynamic study has been performed by Billing et al. [49]-[52]. A semi-classical theory, for the interaction of molecules with a non rigid surface, has been developed and applied to the $H_2(v,j)/Cu(100)$ system. In the dynamics the interaction mechanism assumes the excitation of both the surface phonons and the electrons to be treated within a quantum approximation.

Table III shows the dissociation probability for H_2 colliding with a Cu surface as a function of initial internal vibrational excitation and kinetic energy. We see that the dissociation probability increases with the vibrational excitation such that the kinetic energy threshold is lowered considerably with the vibrational energy. The table also shows that the rotational-vibrational quenching of an H_2 molecule leaving the surface is modest if not null. Also, the energy transfer to the phonons is small due to the small mass of the H atom compared with the Cu mass. These results completely contradict those by Karo *et al.*, even though the surfaces examined by the two groups (Fe/Cu) are different.

Interesting results have been also obtained for the recombination process of atomic hydrogen on Cu. Experimental results established by Hall *et al.* [53] and by Eenshuistra *et al.* [54] showed highly non equilibrium vibrational distributions of H_2 coming from the heterogeneous recombination process.

Two mechanisms are usually invoked to explain the recombination process i.e., the Eley-Rideal (*E-R*) and the Hinshelwood-Langmuir (*H-L*) ones.

According to the *E-R* mechanism the recombination occurs between an atom in the gas phase and an adsorbed atom on the surface. The atom on the surface can be physisorbed or chemisorbed. In the first case the total available energy is given by the dissociation energy of the molecule added to the initial energy of the incoming atom. For the chemisorbed atom we should subtract the binding energy, about 2.5 eV. The *E-R* mechanism can yield vibrationally excited molecules in the whole vibrational manifold for physisorbed atoms and up to $v = 4$ for chemisorbed atoms.

TABLE III

Dissociation Probabilities And Energy Accomodation For $H_2(\nu, j)$ Colliding With A Cu(100) Surface As A Function Of Vibrational And Rotational Angular Momenta ν And j And Initial Kinetic Energy

ν	j	E_{kin} (eV)	P_D ^{a)}	ν' ^{b)}	j' ^{b)}	$E^{int\ b,c)}$ (eV)
5	0	1,0	0,0	5	0,1	0,016
		2,0	0,70	5	1	0,026
6	0	0,2	0,0	6	0,1	0,0024
		0,4	0,0	6	0,1	0,0060
		0,6	0,0	6	1	0,0095
		1,0	0,62	6	1	0,014
8	0	0,05	0,0	8 (7)	0	0,001
		0,2	1,0			
10	0	0,05	0,95			
		0,1	1,0			

^{a)} Dissociation probability.

^{b)} Averaged values for reflected trajectories.

^{c)} Energy transferred to surface phonons.

The *H-L* mechanism considers the recombination process as occurring through two chemisorbed atoms. In this case, the available energy can pump only the first vibrational excited level of the desorbing molecule.

The semiclassical molecular dynamics approach developed by Billing *et al.* has been used to calculate the recombination rate of H and D atoms on copper surfaces according to the *E-R* mechanism (see Fig. 10). The authors considered the case of physisorbed atoms. Of special interest is the final state distribution on vibrational and rotational levels. Figs. 11 and 12 show the normalized contributions to the reaction rate constant, for hydrogen and deuterium recombination as a function of the vibrational states of the nascent molecule, at a temperature of 5000 K. For hydrogen molecules, about 50% have ν less than 5. Due to the smaller vibrational spacing in deuterium, higher vibrational quantum numbers are accessible with a given amount of energy and hence about 80% of the molecules desorbs with ν less than 7.

The *E-R* mechanism has been also studied, by other authors, on copper and tungsten surfaces [55], [56] obtaining results similar to those described by Billing *et al.* On the other hand, a study by Shalashilin *et al.*, on the *E-R* mechanism of H impinging on chemisorbed D on Cu and vice-versa, shows an excitation of desorbed molecules up to $\nu = 3$ [57].

The recombination of atomic hydrogen on graphite has been recently analyzed by our group and is reported in Appendix 1.

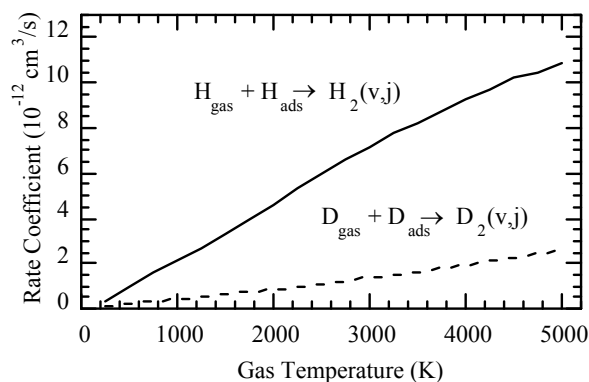


Fig. 10 Recombination rates for H₂ and D₂ versus gas temperature. The surface temperature is 300 K [52].

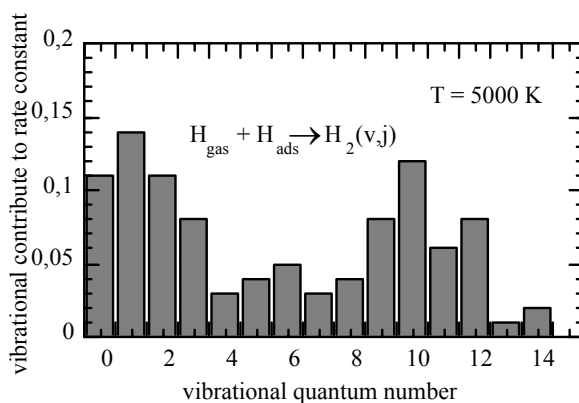


Fig. 11 Normalized vibrational contribute to the recombination reaction rate constant for H₂ (adapted from [52]).

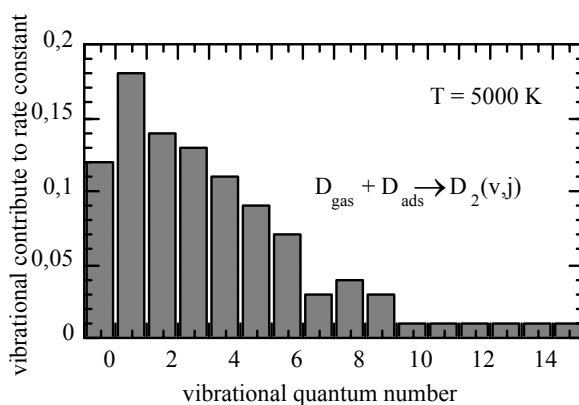


Fig. 12 Normalized vibrational contribute to the recombination reaction rate constant for D₂ (adapted from [52]).

8. Conclusions

We have presented, in the previous pages, the efforts made, in the past, to understand the physics of negative ion sources. Nowadays, different groups are actively working to understand the formation of negative ions in parallel plate rf reactors [58], [59], in flowing rf inductive discharges [60]-[62], in glow discharges [63] as well as in low voltage Cs-H₂ discharges [64], [65] (see Appendix 2 for the recent efforts made by our group [95]). On the other hand, other groups are interested on the influence of negative ions on the so called molecule assisted recombination, for conditions typical of divertor plasmas [66]-[68]. All these groups could join their efforts for better understanding negative ion sources, for the next ITER project.

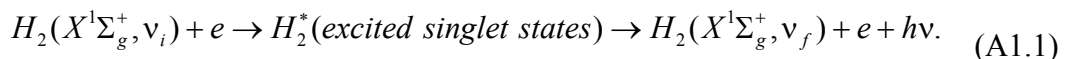
We believe in fact, that further work needs to completely understand the physics of negative ions. We should add to the list of the unresolved problems, discussed in the previous pages, also the problem of transforming the existing sophisticated zero dimensional codes [69], [70] into *1D/2D* codes. The existing dimensional codes, that take into account the transport of vibrationally excited molecules and of negative ions in the source, use, generally, quite simplified kinetic models, so losing a lot of information about the production of negative ions. Again, in this case, collaboration between different groups [71]-[73] can help the development of negative ion sources.

Last but not least we should seriously consider to develop a kinetic modeling for understanding the influence of cesium, either in volume discharges or in surface ones, on the enhancement in the production of negative ions.

Appendix 1. Progress in Elementary Processes for Negative Ion Source Modeling

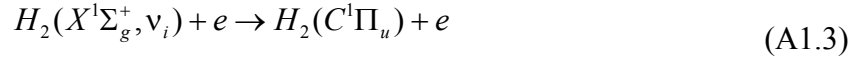
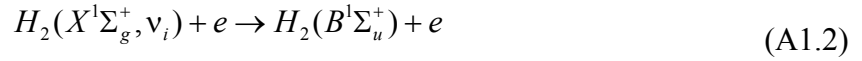
A1.1 Electron-molecule collision processes

Electronic excitation Allowed transitions to the singlet terms of the H₂ spectrum promoted by electron impact have been widely investigated, representing the first step of the indirect mechanism of vibrational excitation, the so-called *E-V process*



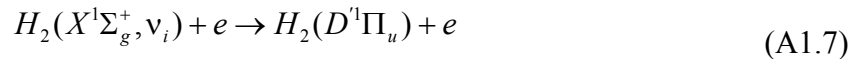
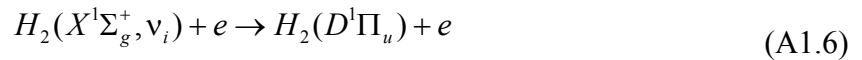
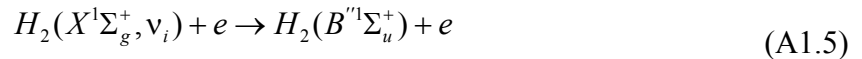
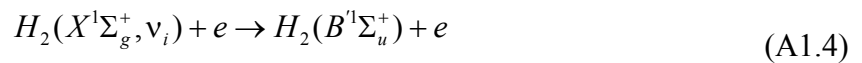
As sketched the fate of excited states is to radiatively decay back to the ground electronic state populating preferentially the high vibrational levels (v_f).

The principal excitations in this excitation-radiative sequence proceed through the lowest singlets $B^1\Sigma_u^+$ and $C^1\Pi_u$ [15]



Total cross sections (summed over final bound and continuum vibrational states) for the processes (A1.2),(A1.3), calculated in the framework of the semiclassical impact-parameter method, have been reported in ref. [15] for H_2 , D_2 , T_2 and DT molecules, as function of both the collision energy and the initial vibrational quantum number. These results allow an interesting study on the existence of isotopic effect. In figure A1.1a the dependence of total cross section on the initial vibrational quantum number for the $X \rightarrow B$ excitation process is presented, at a fixed incident energy, for all isotopic variants of hydrogen molecule. The observed shift of cross sections to higher values of ν_i , in passing from H_2 to T_2 molecule, seems to correspond to the increase of molecular mass. However this isotopic effect is only apparent and the cross sections collapse if plotted as a function of the vibrational eigenvalues (figure A1.1b), suggesting a dependence of excitation cross section on the vertical transition energy.

A not negligible contribution in process (A1.1) is also represented by radiative cascade processes from higher singlet states. Excitations to the B' , B'' , D , D' states, usually referred as low-lying Rydberg states, have been also studied [74]



Total cross sections for processes (A1.4)-(A1.7) are presented in figure A1.2a-d, respectively.

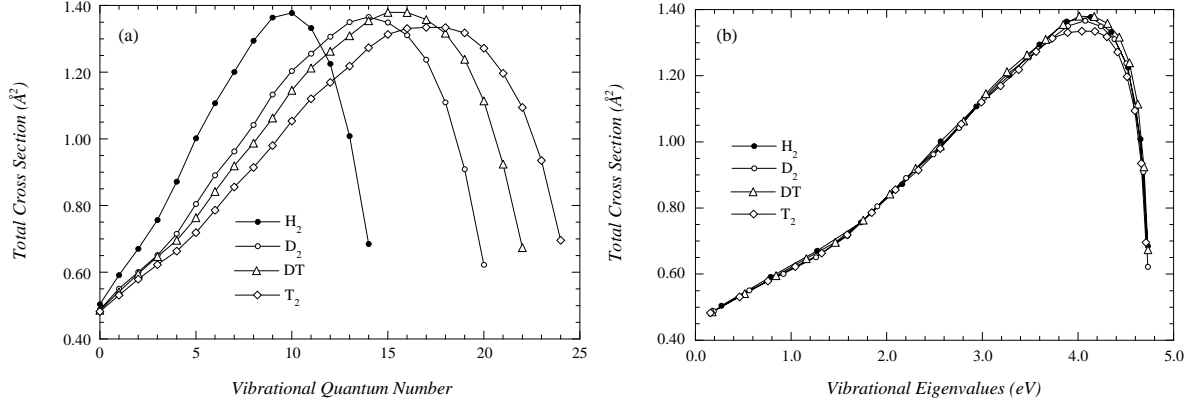


Fig. A1.1. Cross section for the transition $(X^1\Sigma_g^+, v_i) \rightarrow (B^1\Sigma_u^+)$ for different isotopes, at a fixed energy of 40 eV, (a) as a function of initial vibrational quantum number; (b) as a function of vibrational eigenvalues.

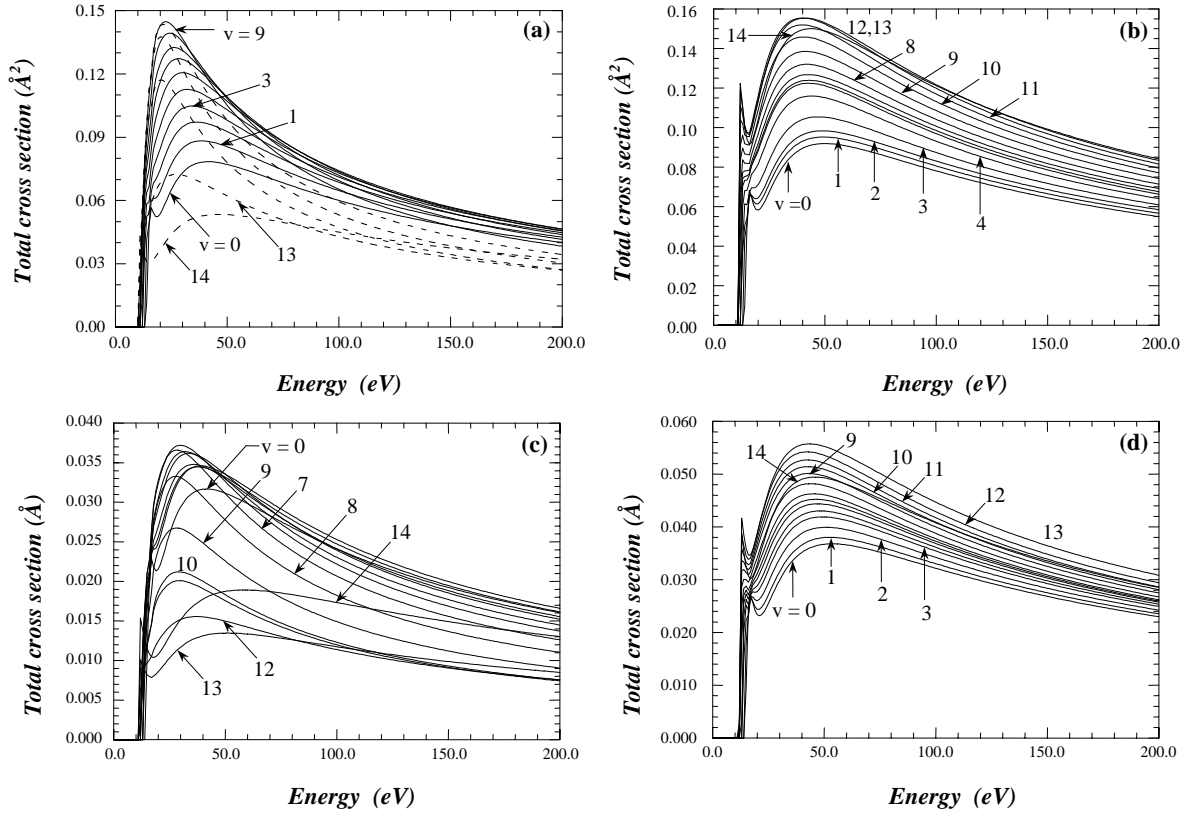


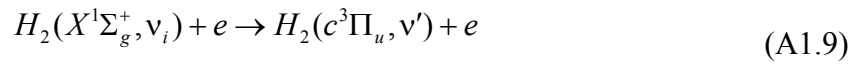
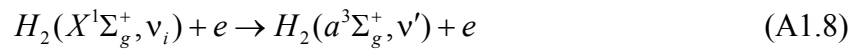
Fig. A1.2. Cross section as a function of energy, for different initial vibrational levels, for the process: (a) $H_2(X^1\Sigma_g^+, v_i) + e \rightarrow H_2(B^1\Sigma_u^+) + e$; (b) $H_2(X^1\Sigma_g^+, v_i) + e \rightarrow H_2(D^1\Pi_u) + e$; (c) $H_2(X^1\Sigma_g^+, v_i) + e \rightarrow H_2(B^1\Sigma_u^+) + e$; (d) $H_2(X^1\Sigma_g^+, v_i) + e \rightarrow H_2(D^1\Pi_u) + e$.

Dissociation The forbidden transition from the ground state to the pure repulsive $b^3\Sigma_u^+$ state represents the main dissociative channel and the related cross sections, for different initial vibrational quantum numbers, have been calculated by different authors [15, 75, 76]. As expected in forbidden transitions the $X \rightarrow b$ cross section is peaked in the threshold region,

while in the high energy region the allowed transitions to the continuum of bound excited electronic states give a significant contribution.

A global dissociative cross section for direct dissociation through excited singlets, including Rydberg states, is reported in figure A1.3. The irregular dependence on the initial vibrational quantum number, determined by the behaviour of Franck Condon density [74, 77], shows that the dissociation is favoured by vibrational excitation.

Transitions populating the vibrational manifold of the lowest bound triplet states (processes (A1.8),(A1.9)) also lead to dissociation through radiative cascade to the b state and predissociation mechanisms, respectively.



State-to-state excitation cross sections, obtained in the Born approximation, summed on the final vibrational manifold, are reported in figure A1.4a-b. The direct dissociation through these states is negligible, this being confirmed by the Franck Condon density evaluation.

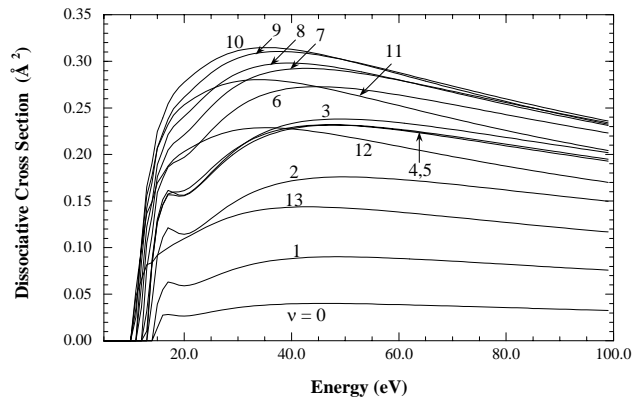


Fig. A1.3. Cross section as a function of energy, for different initial vibrational levels, for the process: $H_2(X^1\Sigma_g^+, \nu_i) + e \rightarrow H_2(B, B', B''^1\Sigma_u^+; C, D, D^1\Pi_u) + e \rightarrow H + H + e$

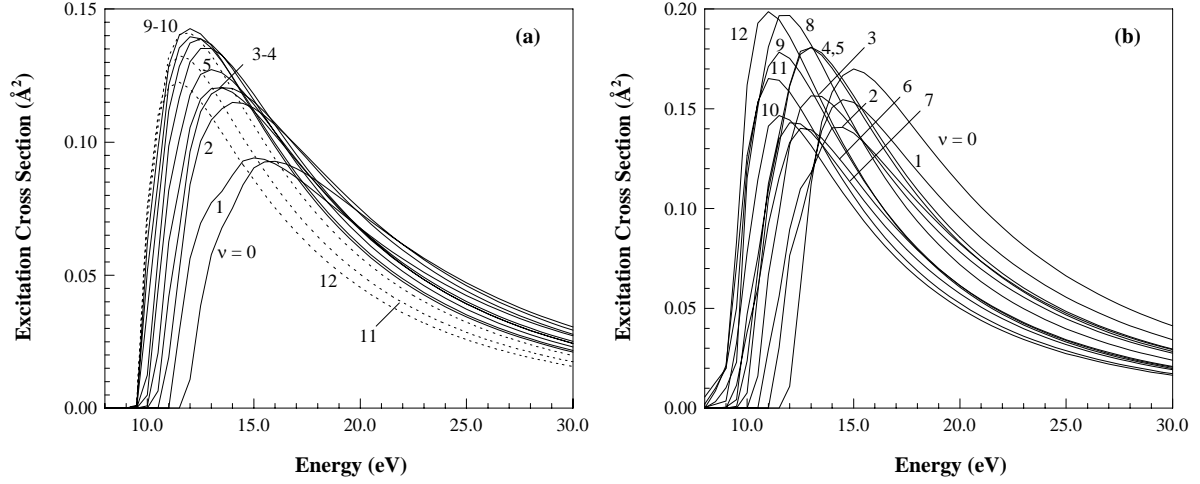
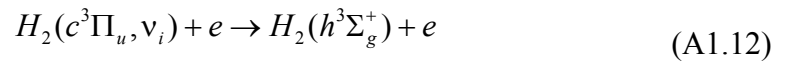
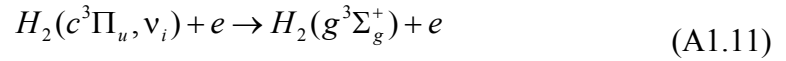
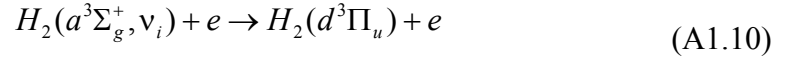


Fig. A1.4. Cross sections as a function of energy for the process (a) $H_2(X^1\Sigma_g^+, \nu_i) + e \rightarrow H_2(a^3\Sigma_g^+) + e$; (b) $H_2(X^1\Sigma_g^+, \nu_i) + e \rightarrow H_2(c^3\Pi_u) + e$.

Triplet-triplet transitions Only few examples of cross section calculations involving two electronically excited states are available in literature, nevertheless these transition can be relevant in plasma modeling. Transitions initiated from the metastable $a^3\Sigma_g^+$ and $c^3\Pi_u$ states to other excited triplet states of H_2 molecules have been considered [77]. In particular process (A1.10), known as Fulcher transition, is important in spectroscopic diagnostic methods, providing information about vibrational and rotational population of hydrogen plasmas [79].



Total cross sections for transitions (A1.10), (A1.11) are shown, as a function of collision energy, respectively in figure A1.5a,b. The relative position of potential energy curves for electronic states does not favour the dissociative channel, which represents a negligible contribution to the total cross sections.

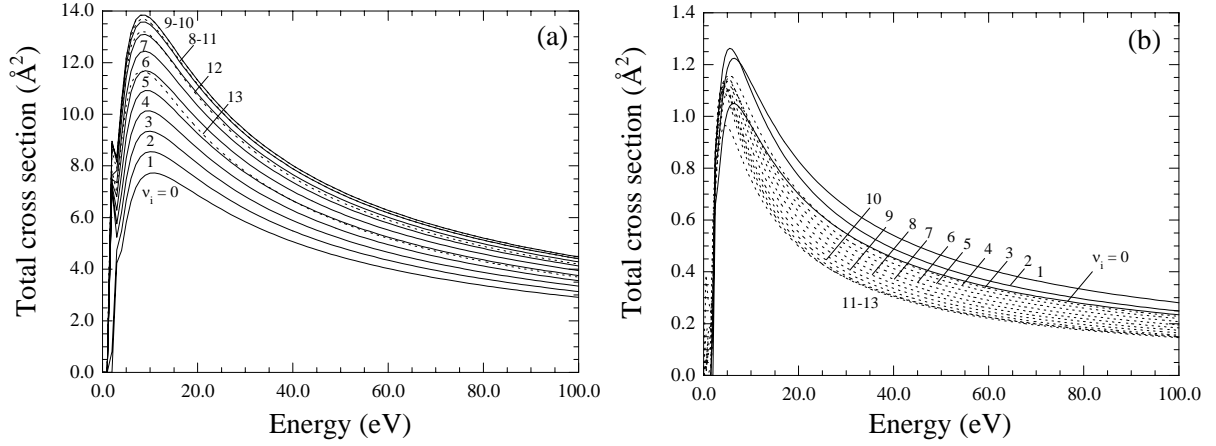


Fig. A1.5. Cross sections as a function of energy for the process (a) $H_2(a^3\Sigma_g^+, v_i) + e \rightarrow H_2(d^3\Pi_u) + e$; (b) $H_2(c^3\Pi_u, v_i) + e \rightarrow H_2(g^3\Sigma_g^+) + e$.

A special treatment is required for the transition to the $h^3\Sigma_g^+$ state, whose adiabatic potential energy curve exhibits a barrier sustaining three quasi-bound vibrational levels (Fig. A1.6). These vibrational states, due to their quasistationary character, can lead to dissociation tunneling through the barrier.

Energy positions of quasi-bound vibrational states is determined by using the method of *internal amplitude*, (IA), defined as

$$IA(\varepsilon) = \int_{R_a}^{R_b} \frac{|\Psi_\varepsilon(R)|^2 dR}{[R_b - R_a]} \quad (\text{A1.13})$$

(R_a and R_b are the two classical turning points of the vibrational energy level). The IA is shown in figure A1.7 as a function of the potential energy ε . The peaks indicate three regions of resonances which, except for the last one very close to the top of the barrier, present a very sharp intensity. At a closer resolution becomes evident the energy enlargement, as shown in the inserted picture in figure A1.7. In figure A1.6 are shown the vibrational wavefunctions of three quasi-bound states, at a selected energy corresponding to the maximum of the related IA . In the same plot the dotted line represents, as a comparison, the wavefunction of completely dissociative state. The cross sections for these states depend on the ratio between the tunneling and radiative times. The calculated values (obtained by evaluating the tunneling probabilities and radiative Einstein coefficients) are shown in figure A1.8. As expected, the last resonance, located at the maximum of the barrier, shows a strong dissociative character,

being the contrary for the first state, placed inside the potential well, which behaves practically as a bound state. An ibrud character is displayed by the second resonance.

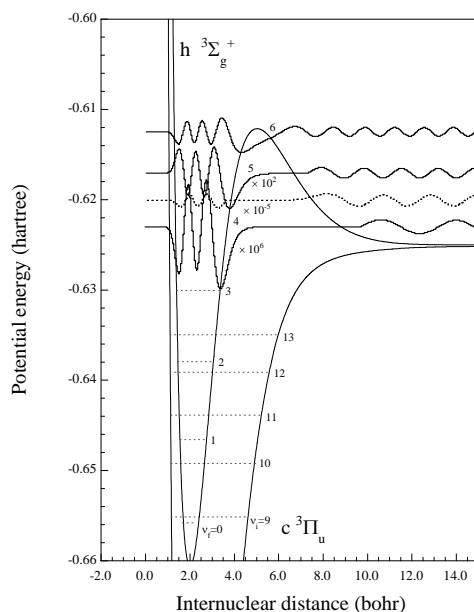


Fig. A1.6. Potential energy curves and vibrational levels for $c^3\Pi_u$ and $h^3\Sigma_g^+$ states of H_2 . Some wavefunctions of quasi-bound states (corresponding to Internal Amplitude peaks) (full lines) and for a non quasi-bound level (dashed line) are also displayed. The left portion of the first three wavefunctions has been multiplied by 10^{-6} , 10^5 (dashed line) and 10^{-2} for a better representation.

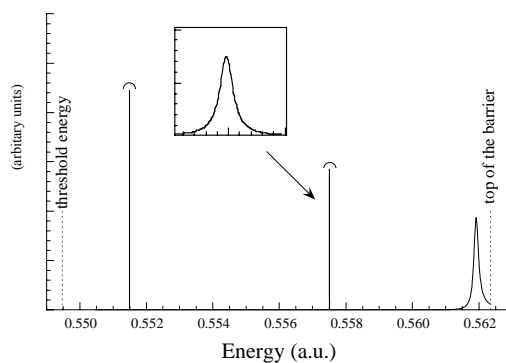


Fig. A1.7. Internal amplitude (A1.13) as a function of continuum energy (the second peak is magnified in the inserted picture).

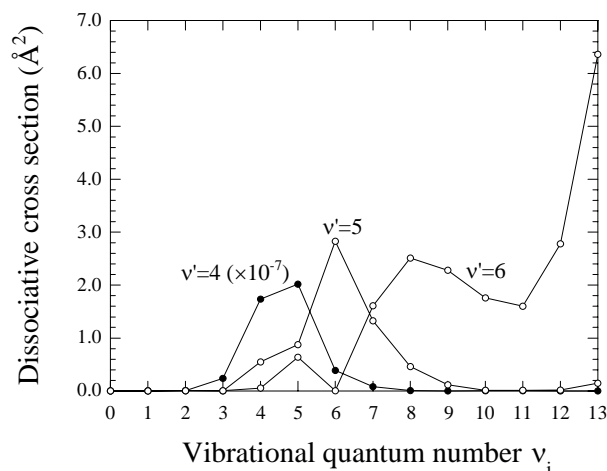


Fig. A1.8. Quasi-bound state dissociative cross section for the process $H_2(c^3\Pi_u, v_i) + e \rightarrow H_2(h^3\Sigma_g^+, v') + e$ as a function of initial vibrational quantum number, at the incident energy $E=10$ eV. The curve labeled as $v'=4$ has been multiplied by a factor of 10^7 .

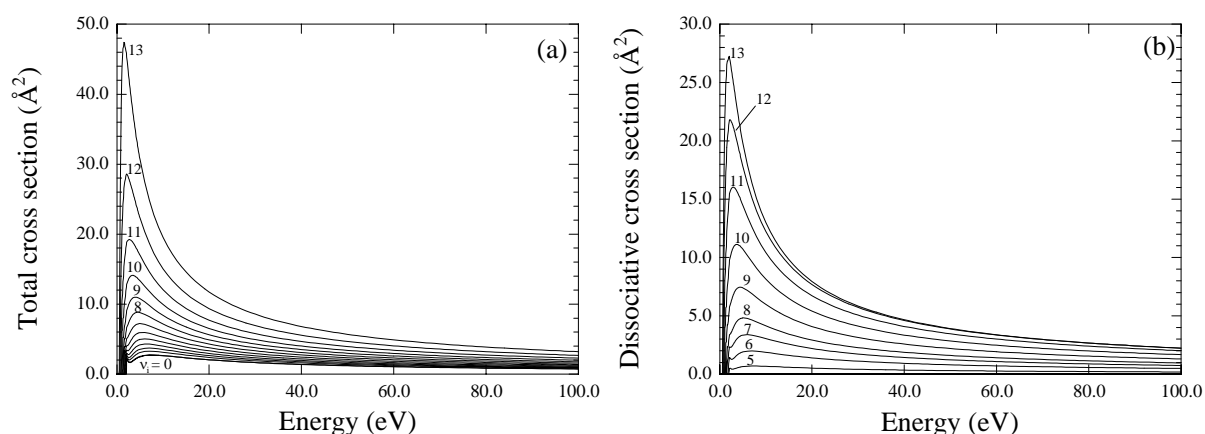


Fig. A1.9. Cross sections as a function of energy for the process (a) $H_2(c^3\Pi_u, v_i) + e \rightarrow H_2(h^3\Sigma_g^+) + e$; (b) $H_2(c^3\Pi_u, v_i) + e \rightarrow H_2(h^3\Sigma_g^+, v) + e \rightarrow H + H + e$.

Total and dissociative cross sections for $c \rightarrow h$ transition, as a function of the energy and the initial vibrational quantum number, are presented in figure A1.9.

A1.2 Atom-molecule collision processes

Extensive dynamical calculations have been performed [18, 94] on the LSTH (Liu-Siegbahn-Truhlar-Horowitz) PES [80] of state-to-state (*VT-processes*) and dissociation cross sections for collision of atomic hydrogen with rovibrationally excited molecular hydrogen.

All possible molecular rovibrational states (348) relative to the used PES have been considered and used as initial states, including quasibound ones (classically bound but quantumly subject to tunnelling), which are of importance for recombination kinetics.

The code integrates the Hamilton equations of motion using Runge-Kutta fourth-order method with variable time step size controlled by a space interval of 0.015 Å and a velocity interval of 0.01 Å/fs. Total energy error checks (6×10^{-4} eV) are also performed. The impact parameter is scanned using a stratified sampling method. The standard QCT method (quasiclassical trajectory method) has been modified by using continuous distributions of rovibrational actions in reactants instead of delta function distributions, weighting trajectories with a simple "square window" function centered in integer values with integer width [81]. Dissociative cross sections as a function of the relative collision energy for different (v, j) pairs are presented in figure A1.10.

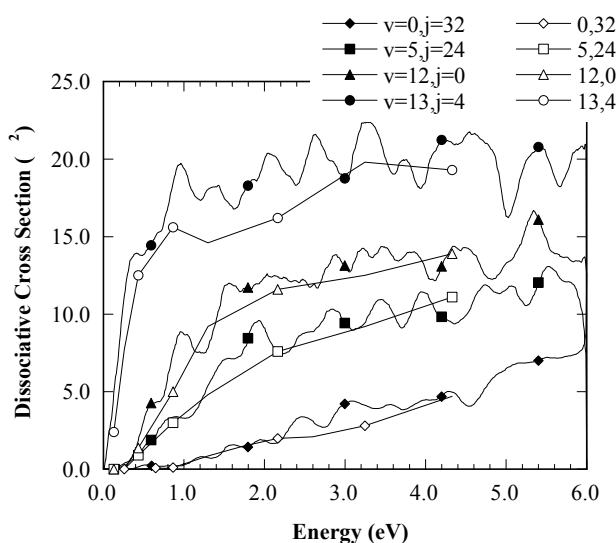
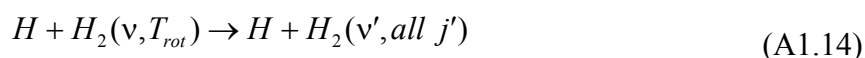


Fig. A1.10. Dissociative cross section for selected initial states of H_2 , as a function of collision energy, compared with results of ref. [82] (open symbols).

Cross section energy profile is characterized by a threshold energy, decreasing with the target internal energy, and by an increasing trend up to a maximum, whose value strongly depends on the initial roto-vibrational state. Comparing the cross sections with results calculated with a similar approach for few transitions by Dove and Mandy [82] (also reported in figure A1.10) a good agreement is found.

State-selected dissociative rate coefficients, $K_d(v)$, (figure A1.11) have been obtained from cross section data, averaging on a Boltzmann distribution function of the rotational states.

Cross sections for vibrational de-excitation process



summed over final j' values and averaged on the rotational temperature, have been obtained including both reactive and non-reactive collisions. The cross section sharply increases with translational energy up to a maximum and then decreases to an approximately flat trend. In figure A1.12a-b results for monoquantic de-excitation initiated from two different vibrational levels are shown for different rotational temperatures. Vibrational excitation emphasizes the peak value and shifts its position in the low energy region. The cross section dependence on the rotational temperature is more significant for low initial v , due to the wide rotational ladder and to the related large contribution at high rotational temperature. Derived rate coefficients are in good agreement with the rates calculated by Laganá [83].

In order to compare the calculated dynamical data with experimental results, the global dissociation rate coefficient has been derived, building up a kinetic model of the H_2 dissociation as occurring in a thermal bath of atoms at a temperature T . The atomic hydrogen concentration is taken to be 100 times higher than that one of the molecules. As a consequence only V-T processes involving atomic hydrogen can be assumed to significantly contribute to populate the vibrational ladder. The kinetic problem deals with the solution of the vibrational master equation including 15 vibrational levels of H_2 submitted to the action of processes



In this scheme the global dissociation rate is the resultant of the dissociative processes initiated from vibrationally excited molecules, expressed as

$$v_d = N_H \sum_v N_v K_d(v) = N_H N_{H_2} K_d \quad (\text{A1.17})$$

K_d , the second order dissociation constant, can be obtained from the relevant $K_d(v)$ values and from the vibrational distribution function N_v . Vibrational populations have been determined by integration of the system of vibrational master equations, assuming the initial vibrational distribution as a delta function centered at $v=0$ level.

The temporal evolution of vibrational populations can be followed up to the quasistationary condition. Quasistationary vibrational distributions have a markedly Boltzmann character at

all translational temperatures and distortions occur only for high vibrational levels (figure A1.13a). In figure A1.13b the global dissociation constant is displayed as a function of $1/T$, the experimental global dissociation rates quoted in [84] is also reported, showing the good agreement between experimental and theoretical results and indirectly confirming both the accuracy of the potential energy surface and the reliability of the QCT approach.

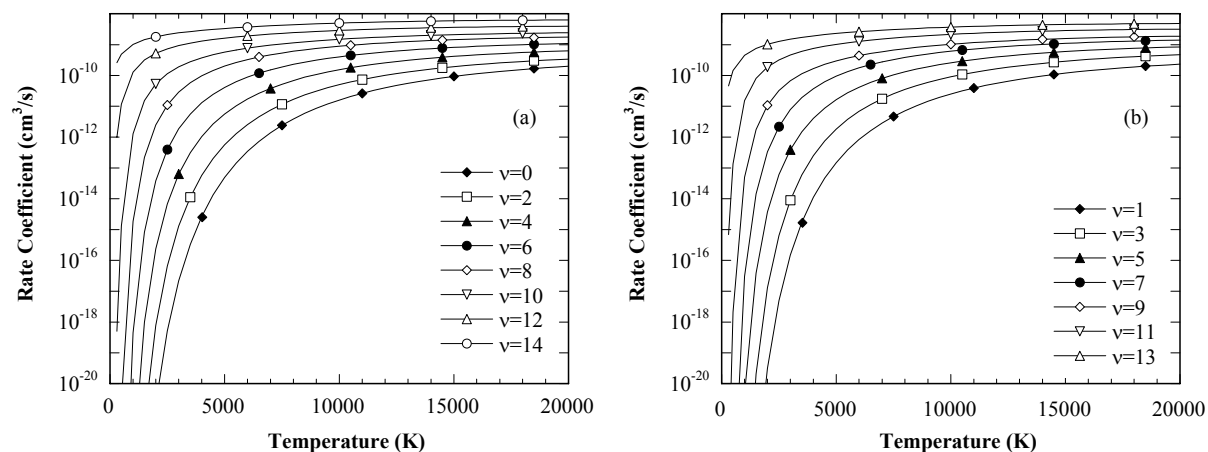


Fig. A1.11. Dissociation rate coefficients averaged over Boltzmann distributions of rotational states plotted as a function of temperature for even (a) and odd (b) vibrational quantum numbers.

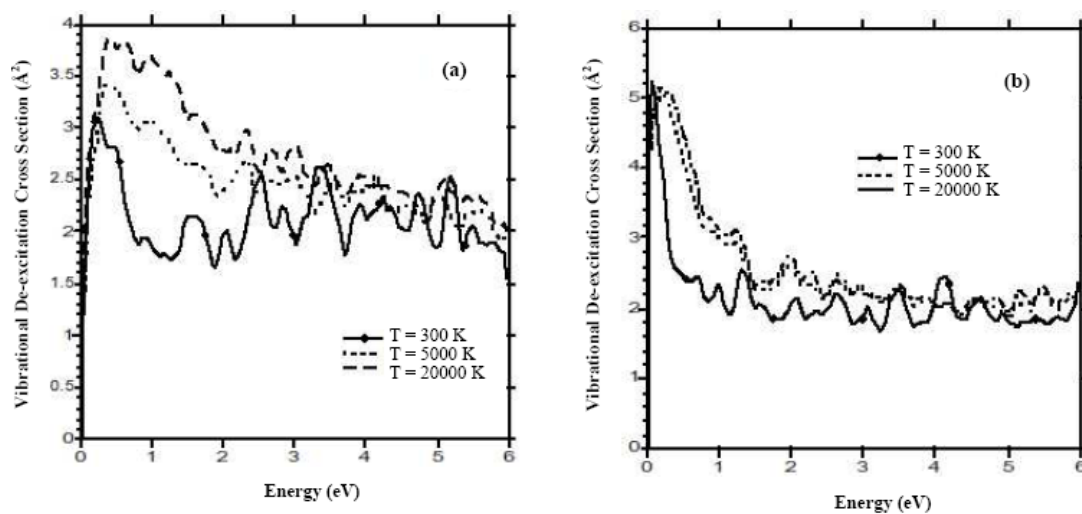


Fig. A1.12. Monoquantic vibrational de-excitation cross sections as a function of translational energy, for different rotational temperatures. (a) $v=5$, (b) $v=9$.

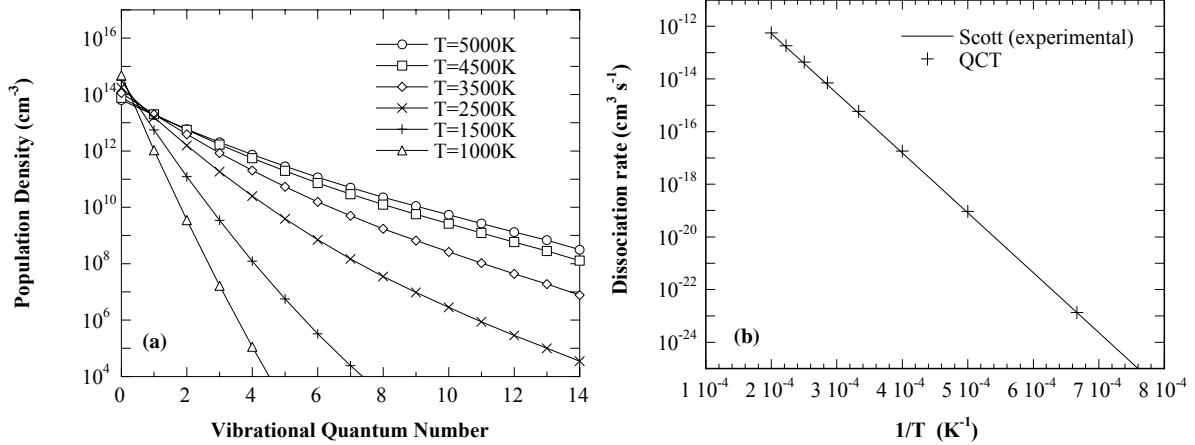


Fig. A1.13. (a) Quasistationary vibrational distribution functions plotted versus vibrational quantum number for different gas temperature values. (b) A comparison of theoretical and experimental values of the global dissociation rate by Scott [84].

A1.3 Surface processes

The interaction of atomic and molecular hydrogen on the reactor walls is relevant in affecting the H_2 vibrational distribution through recombination/dissociation reactions and diffusion processes on the surface.

The recombination of atomic hydrogen on graphite has been studied in the framework of the semiclassical collisional method [85], according to which the dynamics of the chemical particles, H and H_2 , interacting with the graphite surface is described classically by solving the relevant Hamilton's equations of motion while the phonons modes of the graphite surface are treated quantum-mechanically. The coupling between the classical degrees of freedom with the phonons dynamics is made via a time and surface temperature dependent effective potential V_{eff} , of the mean-field type.

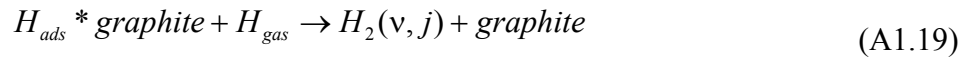
The crystal model K62/62/62 consists of 186 carbon atoms displayed over three layers according to the appropriate lattice symmetry (figure A1.14a).

The adopted hydrogen-surface potential smoothly switches from H_2 -graphite to H -graphite interaction potential according to the $H-H$ interatomic separation. H_2 is physisorbed on graphite in the perpendicular geometry, as confirmed both by experimental and theoretical results [86, 87], the adsorption energy being negligible regardless the adsorption site. On the contrary the H -graphite interaction is characterized by chemisorption, the binding energy depending on the interacting site. Different semiempirical electronic structure calculations have been performed to explore the potential surface and it turns out that the strongest interaction occurs on top of carbon atom, i.e. at the lattice site A in figure A1.14b. The interaction potential for atomic hydrogen approaching the surface perpendicularly at site A

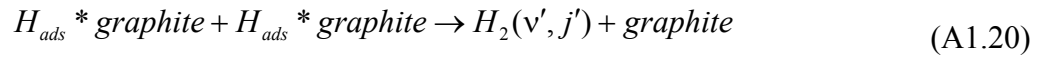
has been modelled fitting results by Fromhertz et al. [88] (figure A1.15a) and by Jeloica et al. [89] (figure A1.15b).

The more recent DFT calculations performed by Jeloica et al. predict a well depth a factor two lower with respect to the value of ref. [88], affecting significantly the catalytic activity of the graphite surface. Reported results have been obtained employing the potential by Jeloica et al.. Details on the parametric expressions for the interactions potentials can be found in refs. [90, 91]. Hydrogen recombination at graphite surface can occur through two alternative mechanisms:

- the direct Eley-Ridell two-step mechanism (*E-R mechanism*)



- the indirect Langmuir-Hinshelwood mechanism (*L-H mechanism*)



The L-H mechanism simulation of the diffusive processes of adsorbed hydrogen atoms across the surface is complex and requires the knowledge of the full topology of the interaction potential, therefore the E-R recombination reaction has been studied.

The adsorbed H atom is placed at the equilibrium distance of 1.5 Å and in thermal equilibrium with the surface at the temperature T_S , the molecular dynamic code simulates the H atom in the gas phase impinging on the surface with polar angles $(\theta; \phi)$ with a kinetic energy E_{kin} , giving the recombination probabilities, the nascent vibrational and rotational distribution of formed H_2 molecules and reaction probabilities for different reaction products. Recombination probability critically depends on surface temperature: the increase of T_S corresponds to the decrease of the probability for the recombination. It can be appreciated by inspection of figure A1.16 where results for $T_S = 10K$ (temperature range for astrophysical applications) and for $T_S = 500K$ are presented. The energy distribution analysis shows that a fraction of the exothermic energy released in hydrogen recombination is shared among the internal states of the newly formed molecules, leading to non-Boltzmann nascent vibrational distribution, being the non-equilibrium character emphasized at high surface temperature. In

figure A1.17 typical calculated vibrational populations of H_2 molecules for different surface temperatures are presented, at the impact energy of 0.03 eV.

The interaction with graphite actually can lead to activation of several reaction exit channels:



the non-reactive surface processes (A1.21)b-d are relevant in the investigation of plasma walls performance in fusion devices, in fact the relative importance with respect to the recombination channel can be considered as an indication of the efficiency of surface damage processes experimentally observed. Probabilities for reactive and non-reactive channels in hydrogen-graphite interaction are presented in figure A1.18.

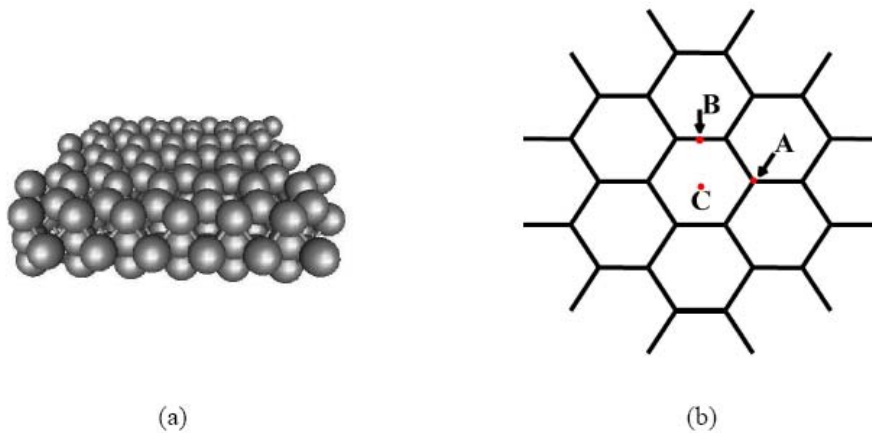


Fig. A1.14. (a) Crystal model K62/62/62. (b) Graphite surface structure.

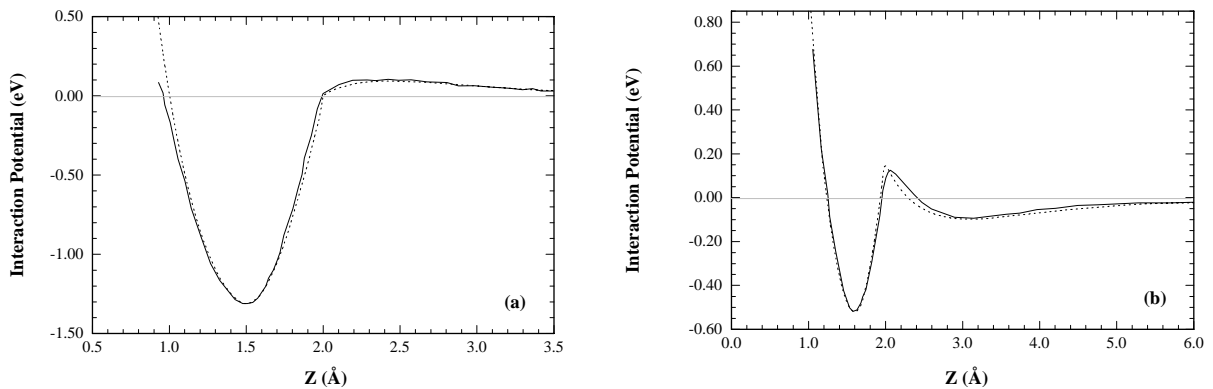


Fig. A1.15. Hydrogen-surface interaction potential as a function of the atom surface distance, Z , at the site A . (a) ref. [88], (b) ref. [89]; dashed lines indicate fitting curves.

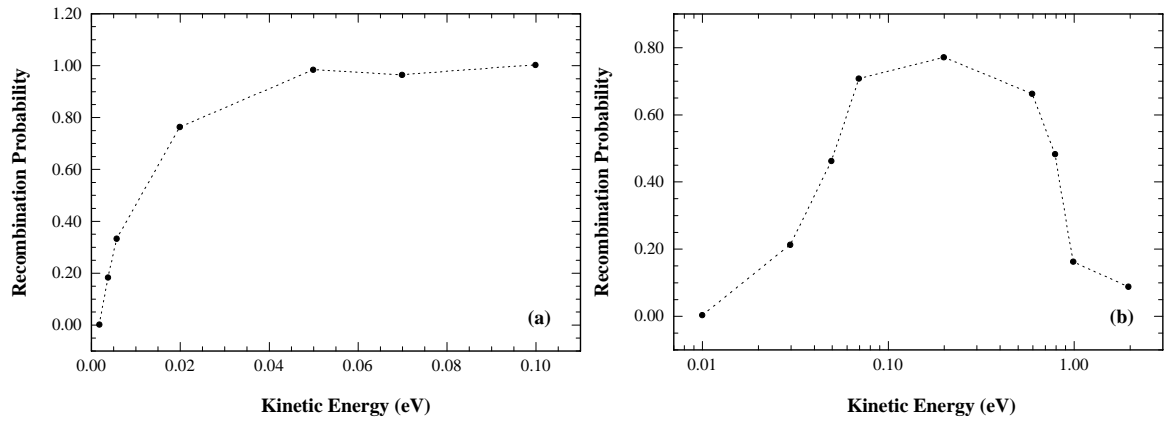


Fig. A1.16. Recombination probability as a function of incident kinetic energy. (a) $T_S = 10K$; (b) $T_S = 500K$.

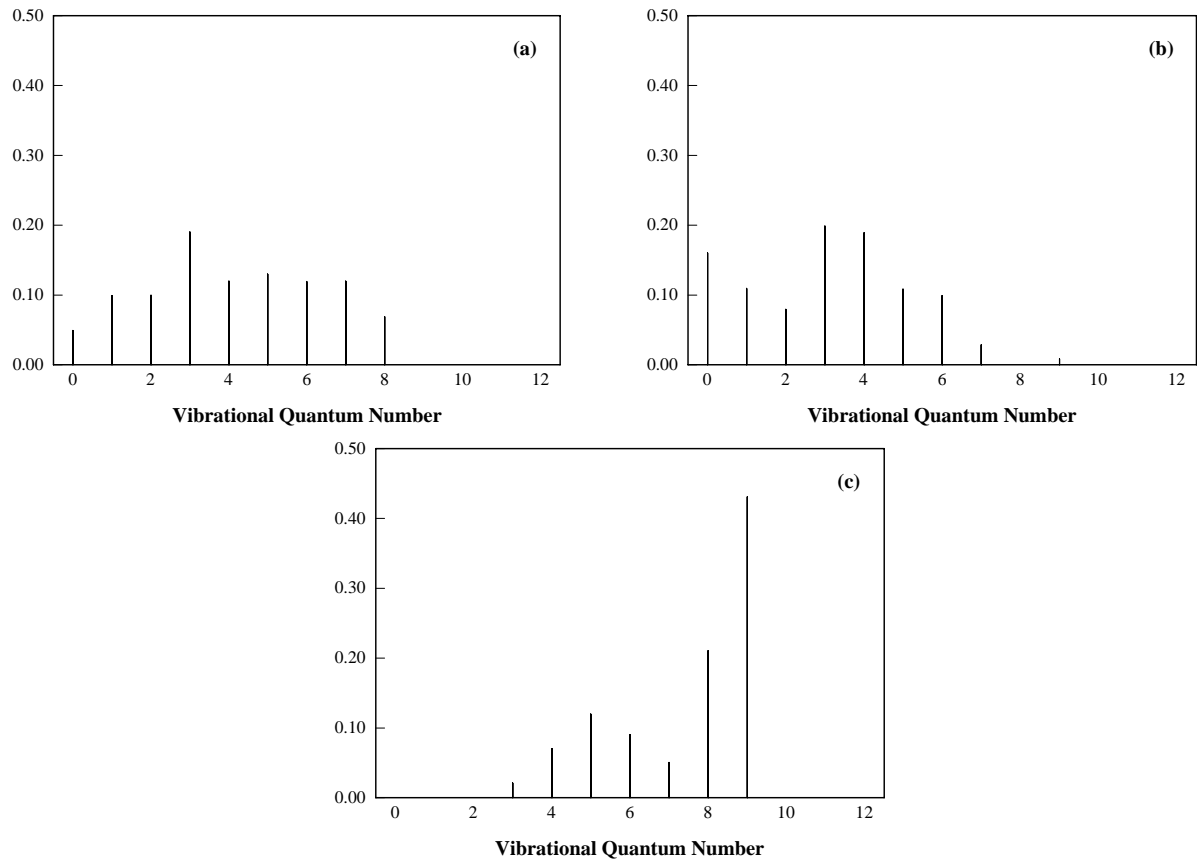


Fig. A1.17. Population of vibrationally excited H_2 molecules in recombination process at the impact energy of 0.03 eV. (a) $T_S = 10K$; (b) $T_S = 100K$; (c) $T_S = 500K$.

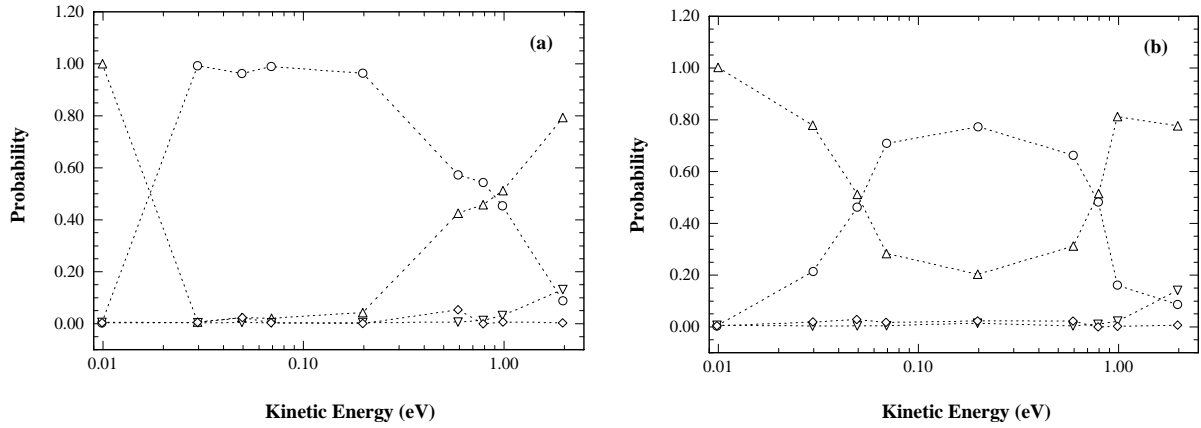


Fig. A1.18. Probability for recombination (circles), adsorption of one atom (triangles), of both atoms (diamonds) and scattering of both atoms (down triangles) as a function of incident kinetic energy. (a) $T_S = 100K$; (b) $T_S = 500K$.

Appendix 2. Recent achievements in modelling for negative ion sources

Different methods can be used to generate plasmas. In this section we consider two different kinds of plasma sources that can be used to generate negative hydrogen ions.

In multicusp ion sources the plasma is produced by high energy electrons, emitted by hot filaments and accelerated by the negative voltage between the filaments and the source wall. The flux of accelerated electrons impinges on the H_2 target and gives rise to molecular and atomic reactions such as ionization, excitation and dissociation. In particular, negative ion production in the plasma volume is driven by the dissociative attachment of low energy electrons to highly vibrationally excited molecules. On the other hand high energy electrons cause H^- destruction through electron detachment. This production mechanism evidences the necessity of dividing the source into two regions where electron energy distributions are optimized respectively for the plasma excitation and the dissociative attachment process. This separation is reached in multicusp ion sources by two kind of “filters”: the first one acts separating spatially electrons with different energies by means of a magnetic filter; the second one, realized pulsing the discharge (temporal filter), creates different electron energy distributions at different times.

Multicusp ion sources present some technical limitations due to the damage of the emitting filaments and their evaporation that causes also a contamination and then a variation in the operating conditions. These problems are absent in a RF discharge: because of their low mass, electrons already present in the gas can be easily accelerated by the electric field to energies which are sufficient to ionize a gas molecule, then generating the plasma.

A2.1 Zero-dimensional Model of Multicusp Ion Sources

In previous works the coupling between heavy particle kinetics and electron kinetics was realized by solving at the same time step on the one hand the master equations describing the temporal evolution of the heavy particle density and on the other one the Boltzmann equation for the electron energy distribution function.

In this section we introduce a new approach [92] to couple heavy particle and electron kinetics, which shows a higher self-consistent character. In our scheme the electron energy range is discretized and represented by a set of intervals. At each interval, characterized by its mean energy, a different “kind” of electron is associated, then these “representative electrons” behave as the vibrationally or electronically excited levels of the hydrogen molecule or atom.

$$n(\varepsilon, t) \approx n(\varepsilon_i, t) \quad \text{for} \quad \varepsilon_i - \frac{1}{2} \Delta\varepsilon_i \leq \varepsilon \leq \varepsilon_i + \frac{1}{2} \Delta\varepsilon_i \quad (\text{A2.1})$$

It means that also for electrons we can write a state-to-state set of kinetic equations whose rate coefficients can be written in the following way:

$$k_i^e = \sigma_i(\varepsilon)v(\varepsilon) \quad (\text{A2.2})$$

which represents the rate coefficient for the excitation of such a species promoted by an electron with velocity:

$$v(\varepsilon) = \sqrt{\frac{2\varepsilon}{m_e}} \quad (\text{A2.3})$$

These rate coefficients are no more global and referred to the overall electron energy distribution function but to an electron with a specific energy.

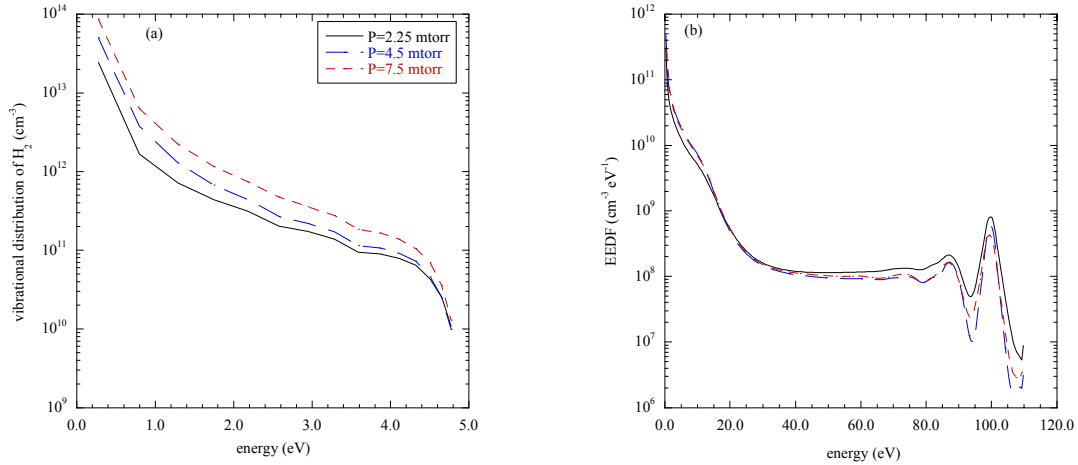


Fig. A2.1. VDF (a) and EEDF (b) for different pressures ($T_g = 500$ K; discharge current = 10 A; discharge voltage = 100 V).

The described approach is easily applicable to all electronic processes, but it can be applied also to describe the flux of electrons along the energy axis due to elastic and electron-electron Coulomb collisions. The numerical scheme resulting from this approach has been used to build a zero-dimensional model of multicusp ion sources in the driver region. The negative ion concentration is described as a function of some discharge parameters (pressure, discharge current) together with electron and heavy particle distributions.

Fig. A2.1a shows the vibrational distribution of H_2 as a function of the vibrational energy for different pressures: increasing the filling pressure, the number density of the vibrational levels increases; low vibrational levels are stronger affected by the increasing pressure. A pressure variation reflects on the plasma potential that governs the electron wall loss: the plasma potential decreases if the discharge current and the voltage current are kept constant. As a consequence the number of low energy electrons increases because they are not lost on the walls (Fig. A2.1b).

A variation of the discharge current does not cause a significant variation of the vibrational distribution of molecular hydrogen (Fig. A2.2a). On the other hand the electron energy distribution function is shifted at higher number density, reflecting the greater number of electrons injected from the filaments (Fig. A2.2b).

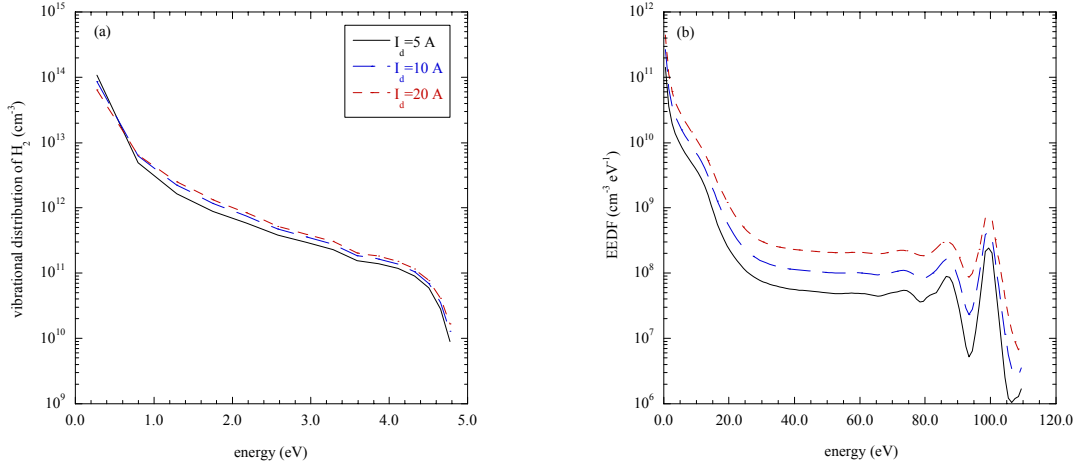


Fig. A2.2. VDF (a) and EEDF (b) for different discharge current ($T_g = 500$ K; pressure = 7.5 mtorr; discharge voltage = 100 V).

A2.2 RF Ion Sources: Inductive discharge

Boltzmann equation assumes a slightly different form when we consider an RF discharge. In this case the source term S is lost, while another one appears, which describes the flux of electrons in the energy space due to the electric field. Then Boltzmann equation reads as [60,61,70]:

$$\frac{\partial n(\varepsilon, t)}{\partial t} = - \left(\frac{\partial J_{el}}{\partial \varepsilon} \right)_{field} - \left(\frac{\partial J_{el}}{\partial \varepsilon} \right)_{e-M} - \left(\frac{\partial J_{el}}{\partial \varepsilon} \right)_{e-e} + In + Ion + Sup - L \quad (A2.4)$$

The integration of the Boltzmann equation requires the determination of the RF electric field amplitude. This amplitude, or the corresponding root mean square (rms) value, can be determined from the absorbed RF power density that is a model input parameter known from the experiment. For this purpose, the following additional algebraic equation that expresses the dependence between the electric field and the absorbed RF power density (RFPD) was coupled to the electron Boltzmann and species balance equations:

$$E_{rms} = \left(MWPD \frac{m_e}{n_e e^2} \right)^{1/2} \left(\int_{\varepsilon} \frac{\nu}{\nu^2 + \omega^2} f(\varepsilon) d\varepsilon \right)^{1/2} \quad (A2.5)$$

where ω is the angular frequency of the RF field, m_e , e , n_e , ε and $f(\varepsilon)$ are the mass, the charge, the density, the energy and the distribution function of electrons, $\nu(\varepsilon)$ is the electron-heavy particle collision frequency.

The model includes a total energy equation that yields the gas temperature that governs the rate constants of the collisions that involve heavy species and a quasi-homogeneous plasma transport model for the estimation of species and energy losses at the plasma reactor wall.

The coupling between all the sub-models is realized through a detailed radiative and collisional model [93].

We analyzed and interpreted vibrational and experimental temperatures of molecular hydrogen obtained by Coherent Anti-Stokes Raman Spectroscopy (CARS) in radiofrequency inductive plasmas in the following discharge conditions: (a) pressure = 1torr, injected power = 0.5W, plasma length = 27cm, radius = 1.27cm, wall temperature = 370K; (b) pressure = 6torr, injected power = 2.0W, plasma length = 27cm, radius = 1.27cm, wall temperature = 550K. We report comparisons between theoretical and experimental vibrational temperatures defined on the basis of the $v = 1$ level to $v = 0$ level population ratio as a function of the recombination factor (Fig. A2.3). Theoretical vibrational temperatures increase with the increase of γ_H .

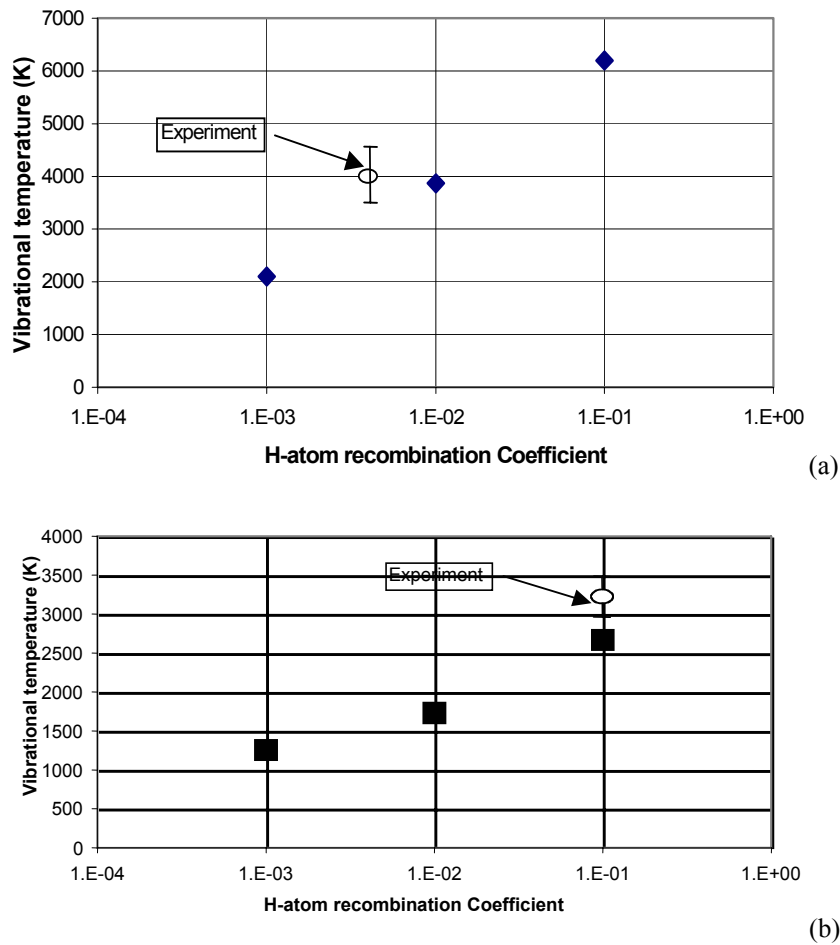


Fig. A2.3. Theoretical vibrational temperature as a function of the atom recombination coefficient. (a) pressure = 1torr, injected power = 0.5W, wall temperature = 370K; (b) pressure = 6torr, injected power = 2.0W, wall temperature = 550K.

The difference in the γ_H values can be partially explained by the different experimental wall temperatures. The variation of the recombination factor reflects obviously on the other features of an RF discharge. In particular increasing γ_H leads to the increase of both the vibrational temperature and the density associated with the plateau of the vibrational distribution (Fig. A2.4).

On the other hand the increase of γ_H results in warming up the EEDF (Fig. A2.5) with a subsequent increase of the electron temperature (Fig. A2.6).

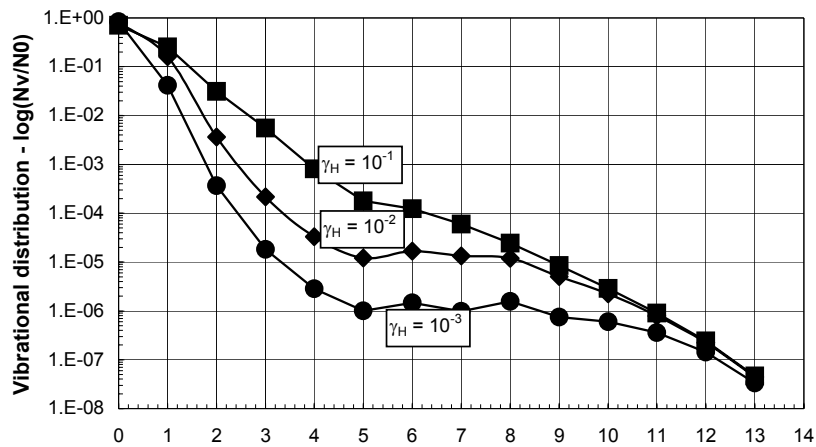


Fig. A2.4. Vibrational distribution functions for different γ_H values.

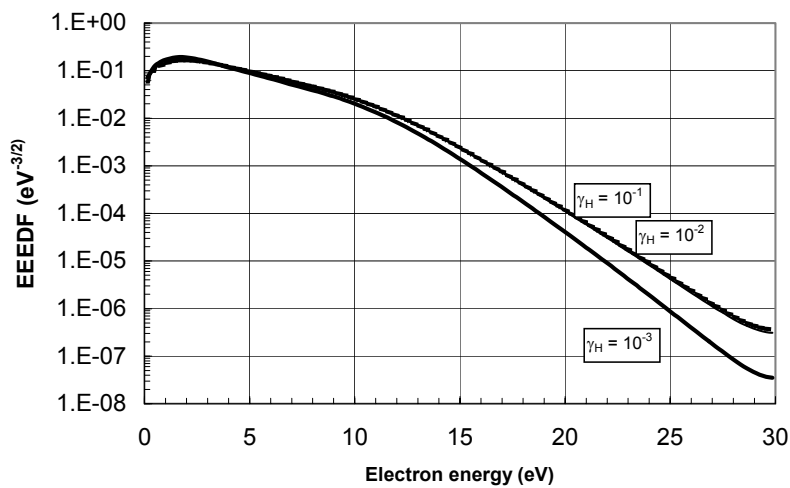


Fig. A2.5. Electron energy distribution function for different γ_H values.

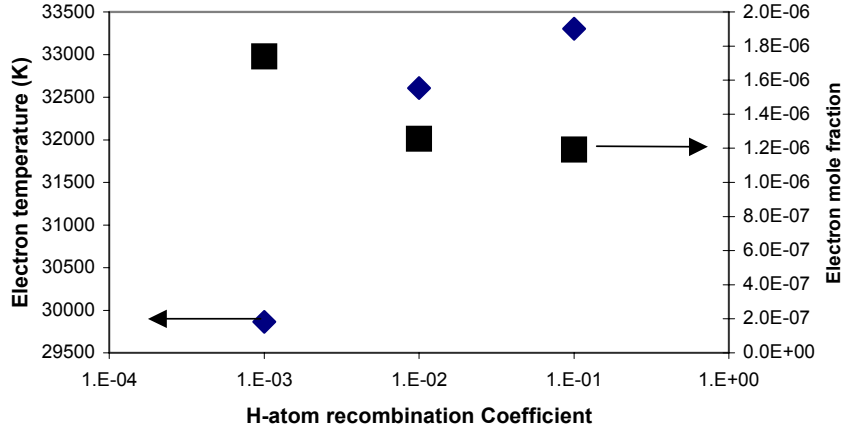


Fig. A2.6. Total electron density and electron temperature as a function of γ_H .

A2.3. 1D(r)2D(v) PIC/MCC Model of RF Parallel Plate Discharges

A 1D(r)2D(v) fully self-consistent particle/continuum model has been developed to study capacitively coupled RF discharge plasmas in hydrogen [58]. The code includes a state-to-state reaction diffusion model.

Also in this case it is necessary to realize a self-consistent coupling of the electron transport with the chemical kinetics, i.e. to solve at the same time the electron transport and chemical kinetics problems taking into account their reciprocal connection.

During the calculations, the densities of different species will be updated by solving appropriate equations. The approach is different for charged and neutral particles.

To solve the problem we use a Particle in Cell/Monte Carlo method for the transport equation and a grid-discretized relaxation technique for the reaction-diffusion part. In the PIC/MCC, applied to electrons and four ionic species (H_3^+ , H_2^+ , H^+ and H^-), the Newton equation for a large ensemble of mathematical point particles is solved taking into account the local electric field as it results from local interpolation within a cell of a mathematical mesh.

The problem can be formalized as follows:

$$\left(\frac{\partial}{\partial t} + v_x \frac{\partial}{\partial x} - \frac{q_s}{m_s} \frac{\partial \varphi(x,t)}{\partial x} \frac{\partial}{\partial v_x} \right) f_s(x, \mathbf{v}, t) = C_s(\{F_c\}) \quad (A2.6)$$

$$\frac{\partial^2 \varphi(x,t)}{\partial x^2} = -\frac{1}{\epsilon_0} \sum_s q_s \int d^3v f_s(x, \mathbf{v}, t) \quad (A2.7)$$

$$-D_c \frac{\partial^2 n_c(x)}{\partial x^2} = \sum_r (v'_{rc} - v_{rc}) k_r \langle f_e \rangle_t \prod_{c'} n_{c'}^{v_{rc}} \quad (A2.8)$$

where f_s and F_c are the kinetic distribution functions for the s -th charged species and the c -th neutral species respectively, q_s and m_s are the s -th species electric charge and mass, φ is the electric potential, n_c is the number density of the c -th neutral component, D_c is its diffusion coefficient, k and ν are, respectively, the rate coefficient and the molecularity of the c -th species in the r -th elementary process.

In eq. (A2.6) C_s is the Boltzmann collision integral for charged/neutral particle collisions:

$$C_s(\{F_c\}) = -f_s(v) \int d^3v' p_{v \rightarrow v'} + \int d^3v' p_{v' \rightarrow v} f_s(v') \quad (\text{A2.9})$$

$$p_{v' \rightarrow v} = \int d^3w d^3w' |v' - w'| \sum_k \sigma_k(v', w', v, w) F_{c(k)}(r, w')$$

where k is an index addressing a specific collision process, σ_k and $c(k)$ are the differential cross section and the neutral collision partner of the k -th process.

The PIC method delivers a solution of the Vlasov-Poisson plasma problem in the following form

$$f_s(\mathbf{r}, \mathbf{v}, t) = \frac{W_s}{N_s} \sum_{p=1}^N S(\mathbf{r} - \mathbf{r}_p) \delta(\mathbf{v} - \mathbf{v}_p) \quad (\text{A2.10})$$

W_s is the ratio between real and simulated particles and S is the particle shape factor which describes the way particles are assigned to the mesh.

The density for the neutral species is obtained by finding a stationary solution for the a set of non-linear equations equal to that given in equation (1) except for a diffusion term that in one dimension reads as:

$$\left(\frac{dN_v}{dt} \right)_{diffus} = D_v \frac{\partial^2}{\partial x^2} N_v \quad (\text{A2.11})$$

After any calculation step of the motion equations, the electric charge in any cell of the mesh is determined from the number of electrons and ions found in the cell itself, according to their statistical weight. Known the electric charge density, the electric potential and field are determined by solving the Poisson equation on the mesh.

The electron-molecule process rates are calculated as a function of the position taking into account the translational non equilibrium of electrons and the vibrational non equilibrium of molecules.

As regard the inclusion of the Boltzmann collision term C_s , as it has been demonstrated [71], a stochastic calculation of C_s in the von Neumann sense delivers directly an improved version of the null-collision Monte Carlo method including the thermal distribution of neutrals.

Recombination processes cannot fit the basic PIC/MCC formalism since they involve two charged particles. These processes are treated as a combination of two first order ones, each including one of the two particle species involved in the process.

The model has been applied to a discharge in pure hydrogen, produced by into a parallel-plate high frequency reactor. One of the plates ($x = 0$) (the so-called “grounded electrode”) is constantly kept at zero voltage, while the other one (the “powered electrode”) is assumed to be driven by an external generator to an oscillating voltage.

We present some results calculated considering the following physical conditions: gas temperature = 300K, voltage amplitude = 300V, gas pressure = 1torr, discharge frequency = 13.56MHz, discharge gap = 0.02m, DC voltage (bias) = 0V.

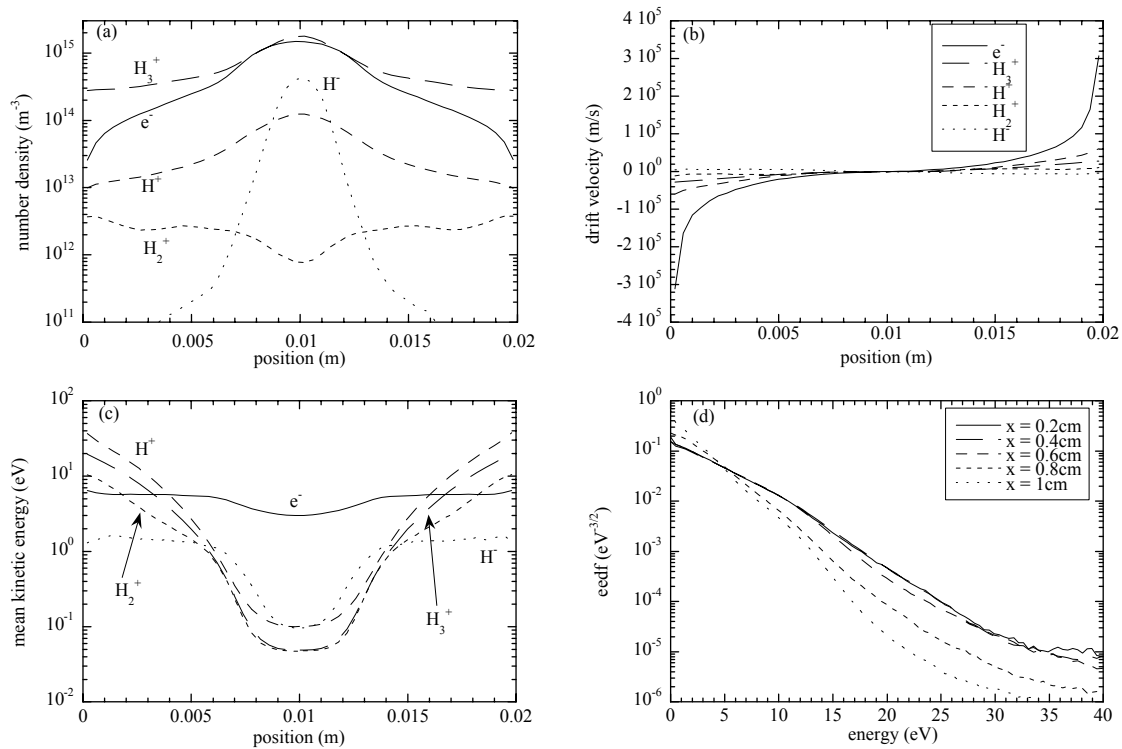
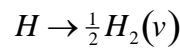


Fig. A2.7. Plasma phase quantities in typical conditions for the probability parameters ($\gamma_v = 0.05$, $\gamma_H = 0.2$): (a) number density, (b) drift velocity, (c) mean kinetic energy of charged species as a function of position and (d) EEDF as a function of energy.

In Fig. A2.7 plasma phase quantities in typical conditions for the probability parameters ($\gamma_v = 0.05$, $\gamma_H = 0.2$) are shown. In particular: (a) number density, (b) drift velocity, (c) mean kinetic energy of charged species as a function of position and (d) electron energy distribution function as a function of energy. From (a) it is evident a slight electronegative behaviour in the centre of the discharge as shown by the separation of the positive ion and electron density in the bulk plasma. The EEDF as shown in (d) significantly deviates from the Maxwell-Boltzmann law showing the necessity of including a kinetic level description of the electron transport.

Table A2.1 reports the results obtained for H^- ions, H atom and electron density varying the vibrational level on which H atoms recombine at the reactor walls, according to the reaction



It can be noticed that the level of recombination has a significant effect on H^- density, while the other quantities are not considerably affected.

Table A2.1. Influence of the vibrational level for H-atom wall recombination.

	n_{H^-} / m^{-3}	n_H / m^{-3}	n_e / m^{-3}
$v = 0$	3×10^{14}	7.3×10^{18}	1.15×10^{15}
$v = 7$	5.72×10^{14}	7.4×10^{18}	1.18×10^{15}
$v = 14$	6×10^{14}	7.4×10^{18}	1.18×10^{15}

Acknowledgements

This work has been partially supported by ASI (I/R/055/02) and MIUR (cof.2003 Project No. 2003037912_010).

References

- [1] M. Bacal, G. W. Hamilton, "H⁻ and D⁻ production in plasmas," Phys. Rev. Lett., vol. 42, pp. 1538-1540, June 1979.
- [2] M. Bacal, G. W. Hamilton, A. M. Bruneteau, H. J. Doucet and J. Taillet, "Measurement of H⁻ density in plasma by photodetachment," Rev. Sci. Instrum., vol 50, pp. 719-721, June 1979.
- [3] J. R. Hiskes, "Cross sections for the vibrational excitation of the H₂(X¹Σ_g⁺) state via electron collisional excitation of the higher singlet states," J. Appl. Phys., vol. 51, pp. 4592-4594, Sept. 1980.
- [4] J. R. Hiskes, A. M. Karo, "Generation of negative ions in tandem high-density hydrogen discharges," J. Appl. Phys., vol. 56, pp. 1927-1938, Oct. 1984.
- [5] J. R. Hiskes, A. M. Karo, P. A. Willmann, "Optimum extracted negative ion current densities from tandem high-density systems," J. Appl. Phys., vol. 58, pp. 1759-1764, Sept. 1985.

- [6] C. Gorse, M. Capitelli, J. Bretagne and M. Bacal, "Vibrational excitation and negative-ion production in magnetic multicusp hydrogen discharges," *Chem. Phys.*, vol. 93, pp. 1-12, Feb. 1985 .
- [7] C. Gorse, M. Capitelli, J. Bretagne M. Bacal and A. Laganà, "Progress in the non-equilibrium vibrational kinetics of hydrogen in magnetic multicusp H- ion sources," *Chem. Phys.*, vol. 117, 177-195, Oct. 1987.
- [8] C. Gorse, R. Celiberto, M. Cacciatore, A. Laganà and M. Capitelli, "From dynamics to modeling of plasma complex systems: negative ion, H⁻ sources," *Chem. Phys.*, vol. 161, pp. 211-227, April 1992.
- [9] J. Bretagne, G. Delouya, C. Gorse, M. Capitelli, M. Bacal, "Electron energy distribution functions in electron-beam sustained discharges: application to magnetic multicusp hydrogen discharges," *J. Phys. D: Appl. Phys.*, vol. 18, pp. 811-825, May 1985.
- [10] J. Bretagne, G. Delouya, C. Gorse, M. Capitelli, M. Bacal, "On electron energy distribution functions in low-pressure magnetic multicusp hydrogen discharges," *J. Phys. D: Appl. Phys.*, vol. 19, pp. 1197-1211, July 1986.
- [11] O. Fukumasa, "Numerical studies on the optimisation of volume-produced H₂ ions in the single-chamber system," *J. Phys. D: Appl. Phys.*, vol. 22, pp. 1668-1679, Nov. 1989.
- [12] R. Keller, R. Thomae, M. Stocklii and R. Welton, "Design, operational experiences and beam results obtained with the SNS H- ion source and LEBT at Berkeley Lab," in *Proceedings of Ninth International Symposium on the Production and Neutralization of Negative Ions and Beams*, Gif-sur-Yvette, France, AIP Conf. Proc., M. R. Stocklii Ed., vol. 639, pp. 47-60, 2002
- [13] J. Peters, "The new HERA H- rf volume source and selected results of plasma investigation," in *Proceedings of Ninth International Symposium on the Production and Neutralization of Negative Ions and Beams*, Gif-sur-Yvette, France, AIP Conf. Proc., M. R. Stocklii Ed., vol. 639, pp. 42-46, 2002.
- [14] W. Kraus, M. Bandyopadhyay, H. Falter, P. Franzen, B. Heinemann, P. McNeely, R. Riedl, E. Speth, A. Tanga, and R. Wilhelm, "Progress in the development of rf driven H⁻/D⁻ sources for neutral beam injection," *Rev. Sci. Instrum.*, vol. 75, pp. 1832-1834, May 2004.
- [15] R. Celiberto, R. K. Janev, A. Laricchiuta, M. Capitelli, J. M. Wadehra, D. E. Atoms, "Cross section data for electron-impact inelastic processes of vibrationally excited molecules of hydrogen and its isotopes," *Atomic Data and Nuclear Data Tables*, vol. 77, pp. 161-213, March 2001.
- [16] M. Capitelli, M. Cacciatore, R. Celiberto, F. Esposito, A. Laricchiuta, M. Rutigliano, "Progress in Elementary Processes for Negative Ion Source Modeling", in *Proceedings of 10th International Symposium on the Production and Neutralization of Negative Ions and Beams*, Kiev. September 14-17 2004, to be published on AIP Conf. Proc. (2005).
- [17] I. Fabrikant, J. M. Wadehra and Y. Xu, "Resonance processes in e-H₂ collisions: dissociative attachment and dissociation from vibrationally and rotationally excited states," *Physica Scripta Volume T*, vol. T96, pp. 45-51, 2002.
- [18] F. Esposito, C. Gorse, M. Capitelli, "Quasi-classical dynamics calculations and state-selected rate coefficients for H+H₂(v,j) to 3H processes: application to the global dissociation rate under thermal conditions," *Chem. Phys. Lett.*, vol. 303, pp. 636-640, April 1999.
- [19] H. Takagi, "Dissociative recombination and excitation of H₂⁺, HD⁺ and D₂⁺ with electrons for various vibrational states," *Physica Scripta Volume T*, vol. T96, pp. 52-60, 2002.
- [20] J. G. Wang, P. C. Stancil, "Hydrogen ion-molecule isotopomer collisions: charge transfer and rearrangement," *Physica Scripta Volume T*, vol. T96, pp. 72-85, 2002.
- [21] M. Pealat, J. P. E. Taran, M. Bacal and F. Hilion, "Rovibrational molecular populations, atoms, and negative ions in H₂ and D₂ magnetic multicusp discharges," *J. Chem. Phys.*, vol. 82, pp. 4943-4953, June 1985.
- [22] P. J. Eenshuistra, R. M. A. Heeren, A. W. Klein and H. J. Hopman, "Dissociation and vibrational excitation of H₂ molecules and wall influence on the densities in a multicusp ion source," *Phys. Rev. A*, vol. A40, pp. 3613-3625, Oct. 1989.
- [23] G. C. Stutzin, A. T. Young, A. S. Schlacher, K. N. Leung and W. B. Kunkel, "In situ measurement of rovibrational populations of H₂ ground electronic state in a plasma by VUV laser absorption," *Chem. Phys. Lett.*, vol. 155, pp. 475-480, March 1989.
- [24] M. Capitelli, C. Gorse, P. Berlemont, D. A. Skinner and M. Bacal, "Theoretical non-equilibrium electron energy distributions of H₂ in magnetic multicusp plasmas: an analysis of the input cross sections data," *Chem. Phys. Lett.*, vol. 179, pp. 48-52, April 1991.
- [25] D. C. Robie, L. E. Jusinski, W. K. Bischel, "Generation of highly vibrationally excited H₂ and detection by 2+1 resonantly enhanced multiphoton ionization," *Appl. Phys. Lett.*, vol. 56, pp. 722-724, Feb. 1990.
- [26] W. G. Graham, "Vacuum ultraviolet emission and H⁻ production in a low pressure hydrogen plasma," *J. Phys. D: Appl. Phys.*, vol. 17, pp. 2225-2231, Nov. 1984.
- [27] O. Fukumasa, Y. Tauchi, Y. Yabuki, S. Mori and Y. Takeiri, "Study of isotope effect on H-/D- volume production in low-pressure H₂/D₂ plasmas using VUV emission," in *Proceedings of Ninth International Symposium on the Production and Neutralization of Negative Ions and Beams*, Gif-sur-Yvette, France, AIP Conf. Proc., M. R. Stocklii Ed., vol. 639, pp. 28-34, 2002

- [28] M. Bacal, M. Glass-Maujean, A. A. Ivanov Jr., M. Nishiura, M. Sasao and M. Wada, "Influence of wall material on VUV emission from hydrogen plasma in H⁻ source," in *Proceedings of Ninth International Symposium on the Production and Neutralization of Negative Ions and Beams*, Gif-sur-Yvette, France, AIP Conf. Proc., M. R. Stocklii Ed., vol. 639, pp. 13-20, 2002.
- [29] T. Mosbach, H. M. Katsch, H. F. Dobele, "In situ diagnostics in plasmas of electronic-ground-state hydrogen molecules in high vibrational and rotational states by laser-induced fluorescence with vacuum ultraviolet radiation," *Phys. Rev. Lett.*, vol. 85, pp. 3420-3423, Oct. 2000.
- [30] T. Mosbach, H. M. Katsch, H. F. Dobele, "Laser Diagnostics of high vibrational and rotational H₂-states," *Contrib. Plasma Phys.*, vol. 42, pp. 650-656, 2002
- [31] M. B. Hopkins and K. N. Mellon, "Enhanced production of negative ions in low-pressure hydrogen and deuterium discharges," *Phys. Rev. Lett.*, vol. 67, pp. 449-452, July 1991.
- [32] M. B. Hopkins, M. Bacal and W. G. Graham, "Enhanced volume production of negative ions in the post discharge of a multicusp hydrogen discharge," *J. Appl. Phys.*, vol. 70, pp. 2009-2014, August 1991.
- [33] H. J. Hopman and R. M. A. Heeren, "Negative ion source technology," in *Plasma Technology : Fundamentals and Applications*, Ed. M. Capitelli and C. Gorse, Plenum New York, pp. 185-201, 1992.
- [34] T. Mosbach, H. M. Katsch, H. F. Dobele., "Temporal behaviour of the H⁻ density in a pulsed multipole discharge investigated by the photodetachment technique," *Plasma Sources Sci. Technol.*, vol. 7, pp. 75-82, Feb. 1998.
- [35] O. Fukumasa and M. Shinoda., "Pulse modulation for plasma parameter control and optimization of volume H⁻ ion source," *Rev. Sci. Instrum.* vol. 69, pp. 938-940, Feb. 1998.
- [36] C. Gorse and M. Capitelli, "Enhanced production of negative ions in low-pressure hydrogen and deuterium pulsed discharges: theoretical calculations," *Phys. Rev. A*, vol. 46, pp. 2176-2177, Aug. 1992.
- [37] C. Gorse, M. Bacal, R. Celiberto and M. Capitelli, "Nonequilibrium plasma kinetics of D₂ in magnetic multicusp plasmas for D⁻ production," *Chem. Phys. Lett.*, vol. 192, pp. 161-165, May 1992.
- [38] J. Bretagne, W. G. Graham and M. B. Hopkins, "A comparison of experimental and theoretical electron energy distribution functions in a multicusp ion source," *J. Phys. D:Appl. Phys.*, vol. 24, pp. 668-671, May 1991.
- [39] O. Fukumasa, N. Mizuki and E. Niitani, "Electron energy dependence of vacuum ultraviolet emission and H⁻ production in a low-pressure hydrogen plasma," *Rev. Sci. Instrum.* vol. 69, pp. 995-997, Feb. 1998.
- [40] W. G. Graham, "The kinetics of negative ions in discharges," *Plasma Sources Sci. Technol.*, vol. 4, pp. 281-292, May 1995.
- [41] O. Fukumasa, S. Mori, N. Nakada, Y. Tauchi, M. Hamabe, K. Tsumori and Y. Takeiri, "Isotope effect of H⁻/D⁻ volume production in low pressure H₂/D₂ plasmas, measurement of VUV emissions and negative ion densities," *Contr. Plasma Phys.*, vol. 44, pp. 516-522, 2004.
- [42] L. A. Pinnaduwege and L. G. Christoforou, "H⁻ formation in laser-excited molecular hydrogen," *Phys. Rev. Lett.*, vol. 70, pp. 754-757, Feb. 1993.
- [43] P. G. Daskos, L. A. Pinnaduwege and J. F. Kielkopf., "Photophysical and electron attachment properties of Ar-F-excimer-laser irradiated H₂," *Phys. Rev. A*, vol. 55, pp. 4131-4142, June 1997.
- [44] A. Garscadden, R. Napgal, "Non-equilibrium electronic and vibrational kinetics in H₂-N₂ and H₂ discharges," *Plasma Sources Sci. Technol.*, vol. 4, pp. 268-280, May 1995.
- [45] C. Gorse, M. Capitelli, R. Celiberto, D. Iasillo and S. Longo, "Recent Advances in H₂/D₂ plasma kinetics," in *Proceedings of seventh International Symposium on the Production and Neutralization of Negative Ions and Beams*, Upton NV, AIP Conf. Proc., Ed. K. Prelec, vol. 380, pp. 109-115, 1995.
- [46] J. Hiskes, "Molecular Rydberg states in hydrogen negative ion discharges," *Appl. Phys. Lett.*, vol. 69, pp. 755-757, Aug. 1996.
- [47] K. Hassouni, A. Gicquel, M. Capitelli, "The role of dissociative attachment from Rydberg states in enhancing H⁻ concentration in moderate and low pressure H₂ plasma sources," *Chem. Phys. Lett.*, vol. 290, pp. 502-508, July 1998.
- [48] L. A. Pinnaduwege, W. X. Ding, D. L. McCorkle, S. H. Lin, A. M. Mebel, A Garscadden, "Enhanced electron attachment to Rydberg states in molecular hydrogen volume discharges," *J. Appl. Phys.*, vol. 85, pp. 7064-7069, May 1999.
- [49] M. Cacciatore and G. D. Billing, "Dissociation and atom recombination of H₂ and D₂ on metallic surfaces: a theoretical survey," *Pure Appl. Chem.*, vol. 68, pp. 1075-1081, 1996.
- [50] G. D. Billing and K. V. Mikkelsen, "Advanced Molecular Dynamics and Chemical Kinetics," John Wiley & Sons, New York, 1997.
- [51] M. Cacciatore, M. Capitelli and G. D. Billing, "Relaxation dynamics of vibrationally highly excited H₂ molecules on a Cu surface," *Surf. Sci.* vol. 217, pp. L391-L396, July 1989.
- [52] B. Freiesleben Hansen and G. D. Billing, "Hydrogen and deuterium recombination rates on a copper surface," *Surf. Sci. Lett.*, vol. 373, pp. L333-338, 1997.

- [53] R. I. Hall, I. Cadez, M. Landau, F. Pichou and C. Schermann, "Vibrational excitation of hydrogen via recombinative desorption of atomic hydrogen gas on a metal surface," *Phys. Rev. Lett.*, vol. 60, pp. 337-340, Jan. 1988.
- [54] P. J. Eenshuistra, J. H. Bonnie, J. Los and H. J. Hopman, "Observation of exceptionally high vibrational excitation of hydrogen molecules formed by wall recombination," *Phys. Rev. Lett.*, vol. 60, pp. 341-344, Jan. 1988.
- [55] D. K. Otorbaev, M. C. M. van de Sanden and D. C. Schram, "Heterogeneous and homogeneous hydrogen kinetics in plasma chemistry," *Plasma Sources Sci. Technol.*, vol. 4, pp. 293-301, May 1995.
- [56] B. Jackson and M. Persson, "A quantum mechanical study of recombinative desorption of atomic hydrogen on a metal surface," *J. Chem. Phys.*, vol. 96, pp. 2378-2386, Feb. 1992.
- [57] D. V. Shalashilin, B. Jackson and M. Persson, "Eley-Rideal and hot-atom reactions of H(D) atoms with D(H)-covered Cu(111) surfaces; quasiclassical studies," *J. Chem. Phys.*, vol. 110, pp. 11038-11046, June 1999.
- [58] P. Diomede, S. Longo and M. Capitelli, "Vibrational excitation and negative ion production in Radio Frequency parallel plate H₂ plasmas", *Eur. Phys. J. D*, to be published, 2005.
- [59] B. Kalache, T. Novikova, A. F. Morral, P. R. Cabarrocas, W. Morscheidt, K. Hassouni, "Investigation of coupling between chemistry and discharge dynamics in radio frequency hydrogen plasmas in the torr regime," *J. Phys. D, Appl. Phys.*, vol. 37, pp. 1765-1773, July 2004.
- [60] V. A. Shakatov, O. De Pascale, M. Capitelli, K. Hassouni, G. Lombardi, A. Gicquel, "Measurement of vibrational, gas, and rotational temperatures of H₂ ($X^1\Sigma_g^+$) in radio frequency inductive discharge plasma by multiplex coherent anti-Stokes Raman scattering spectroscopy technique," *Phys. Plasmas*, vol. 12, pp. 23504-1-23504-10, Feb. 2005.
- [61] K. Hassouni, G. Lombardi, A. Gicquel, M. Capitelli, V. A. Shakatov and O. De Pascale, "Non-equilibrium vibrational excitation of H₂ in radiofrequency discharges: a theoretical approach based on Coherent anti-Stokes Raman Spectroscopy (CARS) measurements," *Phys Plasmas*, submitted for publication
- [62] R. Zorat and D. Vender, "Global model for an rf hydrogen inductive plasma discharge in the deuterium negative ion source experiment including negative ions," *J. Phys. D:Appl. Phys.*, vol. 33, 1728-1735, July 2000.
- [63] J. Loureiro, J. Amorim, "Dependence of volume-produced H⁻ ions on the wall recombination probability of H atoms in a low pressure H₂ positive column," *Chem. Phys.*, vol. 232, pp. 141-149, Feb. 1998.
- [64] F. G. Baksht, G. A. Djuzhev, L. I. Elizarov, V. G. Ivanov, A. A. Kostin, S. M. Shkolnik, "Generation of negative hydrogen ions in low voltage caesium-hydrogen discharge," *Plasma Sources Sci. Technol.*, vol. 3, pp. 88-98, Feb. 1994.
- [65] F. G. Baksht, V. G. Ivanov, M. Bacal, "Pumping of highly vibrationally excited molecules in a hydrogen flow through a cesium-hydrogen discharge," *Plasma Sources Sci. Technol.*, vol. 7, pp. 431-439, Aug. 1998.
- [66] S. I. Krasheninnikov, "Molecule assisted recombination, MAR: mechanisms and plasma conditions for effective operation," *Physica Scripta Volume T*, vol. T96, pp. 7-15, 2002.
- [67] A. Yu. Pigarov, "Collisional radiative kinetics of molecular assisted recombination in edge plasmas," *Physica Scripta Volume T*, vol. T96, pp. 16-31, 2002.
- [68] U. Fantz, "Atomic and molecular emission spectroscopy in low temperature plasmas containing hydrogen and deuterium," Max Planck Institute fur Plasmaphysik, IPP-report 10/21, 2001.
- [69] D. Pagano, "Plasma ad idrogeno per la produzione di ioni negativi," Laurea thesis, Chemistry Department, Bari University, Italy, Oct. 1999
- [70] M. Capitelli, O. De Pascale, P. Diomede, A. Gicquel, C. Gorse, K. Hassouni, S. Longo and D. Pagano, "Twenty five years of vibrational kinetics and negative ion production in H₂ plasmas : modelling aspects," in *Proceedings of 10th International Symposium on the Production and Neutralization of Negative Ions and Beams*, Kiev. September 14-17 2004, to be published on AIP Conf. Proc. (2005).
- [71] S. Longo, P. Diomede, "Monte Carlo modeling of gas phase ion transport under thermal gradients and external fields, *Eur. Phys. J. Appl. Phys.*, Vol. 26, pp. 177-185, June 2004.
- [72] A. Hatayama, T. Sakurabayashi, Y. Ishi, K. Makino, M. Ogasawara and M. Bacal, "Development of multidimensional Monte Carlo simulation code for H⁻ ion and neutral transport in H⁻ ion sources," *Rev. Sci. Instrum.*, vol. 73, pp. 910-913, Feb. 2002.
- [73] T. Sakurabayashi, A. Hatayama, K. Miyamoto, M. Ogasawara, and M. Bacal "Monte Carlo simulation of negative ion transport in the negative ion source (Camembert III)," *Rev. Sci. Instrum.*, vol. 73, pp. 1048-50, Feb. 2002.
- [74] R. Celiberto, A. Laricchiuta, U.T. Lamanna, R.K. Janev and M. Capitelli, "Electron-impact excitation cross sections of vibrationally excited $X^1\Sigma_g^+$ H₂ and D₂ molecules to Rydberg states", *Physical Review A*, 60 (1999) 2091.
- [75] T.N. Rescigno and B.I. Schneider, "Electron-impact excitation of the $b^3\Sigma_u^+$ state of H₂ using the complex Kohn method: R dependence of the cross section", *Journal of Physics B* 21 (1988) L691.

- [76] D.T. Stibbe and J. Tennyson, "Near-threshold electron impact dissociation of H₂ within the adiabatic nuclei approximation", *New Journal of Physics* 1, (1998) 21-29.
- [77] R. Celiberto, U.T. Lamanna, M. Capitelli, "Dependence of electron-impact dissociative excitation cross sections on the initial vibrational quantum number in H₂ and D₂ molecules: $X^1\Sigma_g^+ \rightarrow B^1\Sigma_u^+$ and $X^1\Sigma_g^+ \rightarrow C^1\Pi_u$ transitions", *Physical Review A* 50 (1994) 4778.
- [78] A. Laricchiuta, R. Celiberto, and R.K. Janev, "Electron-impact-induced allowed transitions between triplet states of H₂", *Physical Review A* 69 (2004) 022706.
- [79] U. Fantz, B. Heger and D. Wunderlich, "Using the radiation of hydrogen molecules for electron temperature diagnostics of divertor plasmas", *Plasma Physics Controlled Fusion* 43 (2001) 907-918.
- [80] D.G. Truhlar, C.J. Horowitz, "Functional representation of Liu and Siegbahn's accurate *ab initio* potential energy calculations for H+H₂", *Journal of Chemical Physics* 68 (1978) 2466; "Erratum: Functional representation of Liu and Siegbahn's accurate *ab initio* potential energy calculations for H+H₂", 71 (1979) 1514.
- [81] F. Esposito, PhD Thesis, Department of Chemistry, University of Bari (1999).
- [82] J.E. Dove, M.E. Mandy, *Int. J. Chem. Kin.* 18 (1986) 893.
- [83] A. Laganà, E. Garcia, "Quasiclassical rate coefficients for the H+H₂ reaction", University of Perugia, Italy (1996).
- [84] C.D. Scott, S. Fahrat, A. Gicquel, K. Hassouni, M. Lefebvre, *J. Thermophysics and Heat Transfer* 10 (1996) 426.
- [85] G.D. Billing, "Dynamics of molecule surface interactions", Wiley, New York (2000).
- [86] L. Mattera, F. Rosatelli, C. Salvo, F. Tommasini, U. Valbusa, G. Vidali, "Selective adsorption of ¹H₂ and ²H₂ on the (0001) graphite surface", *Surf. Sci.* 93 (1980) 515.
- [87] D. Novaco, J. P. Wroblewski, "Rotational states of H₂, HD, and D₂ on graphite", *Physical Review B* 39 (1989) 11364.
- [88] T. Fromhertz, C. Mendoza, F. Ruetter, *Mon. Not. R. Astron. Soc.* 263 (1993) 851.
- [89] L. Jeloica, V. Sidis, "DFT investigation of the adsorption of atomic hydrogen on a cluster-model graphite surface", *Chemical Physics Letters* 300 (1999) 157.
- [90] M. Rutigliano, M. Cacciatore and G.D. Billing, "Recombination of Hydrogen on a Carbon Surface", *Atomic and Plasma-Material Interaction Data for Fusion*, 9 (2001) 267.
- [91] M. Rutigliano, M. Cacciatore and G.D. Billing, "Hydrogen atom recombination on graphite at 10 K via the Eley-Rideal mechanism", *Chem. Phys. Lett.* 340 (2001) 13.
- [92] D. Pagano, C. Gorse, M. Capitelli, F. Carbutti, "Hydrogen plasmas for negative ion production", *Rarefied Gas Dynamics, 24th International Symposium - RGD24, Monopoli (Bari), Italy 10 - 16 July 2004*, Editor Mario Capitelli, AIP Conference Proceedings 762 (2005) 1151.
- [93] K. Hassouni, A. Gicquel, M. Capitelli, J. Loureiro, "Chemical kinetics and energy transfer in moderate pressure H₂ plasmas used in diamond MPACVD processes", *Plasma Sources Sci. and Technol.* 8 (1999) 494.
- [94] F. Esposito, M. Capitelli, "Dynamical Calculations of State-to-State and Dissociation Cross Sections for Atom-Molecule Collision Processes in Hydrogen", *Atomic and Plasma-Material Interaction Data for Fusion* 9 (2001) 65.
- [95] M. Capitelli, R. Celiberto, O. De Pascale, P. Diomede, F. Esposito, C. Gorse, A. Laricchiuta, S. Longo, D. Pagano, "Elementary processes, transport and kinetics of molecular plasmas", *Atomic and Plasma-Material Interaction Data for Fusion* (2005), in press.